Pre-Steady-State Kinetic Analysis of Processive DNA Replication Including Complete Characterization of an Exonuclease-Deficient Mutant†

Smita S. Patel, Isaac Wong, and Kenneth A. Johnson*

Department of Molecular and Cell Biology, 301 Althouse Laboratory, The Pennsylvania State University, University Park, Pennsylvania 16802

Received February 5, 1990; Revised Manuscript Received August 16, 1990

ABSTRACT: The elementary steps of DNA polymerization catalyzed by T7 DNA polymerase have been resolved by transient-state analysis of single nucleotide incorporation, leading to the complete pathway:

$$E \underset{k_{off}}{\overset{k_{on}[D_n]}{\rightleftharpoons}} E{\cdot}D_n \underset{k_{-1}}{\overset{k_1[N]}{\rightleftharpoons}} E{\cdot}D_n{\cdot}N \underset{k_{-2}}{\overset{k_2}{\rightleftharpoons}} E'{\cdot}D_n{\cdot}N \underset{k_{-3}}{\overset{k_3}{\rightleftharpoons}} E'{\cdot}D_{n+1}{\cdot}P \underset{k_{-4}}{\overset{k_4}{\rightleftharpoons}} E{\cdot}D_{n+1}{\cdot}P \underset{k_{-5}[P]}{\overset{k_5}{\rightleftharpoons}} E{\cdot}D_{n+1}$$

where E, D, N, and P represent T7 DNA polymerase, DNA primer/template, deoxynucleoside triphosphate, and inorganic pyrophosphate, respectively. A DNA primer/template consisting of a synthetic 25/36-mer has been used as a substrate for correct nucleotide incorporation of dTTP in all the experiments. The rate constants and equilibrium constants of each step have been established by direct measurement of individual reactions and fit by computer simulation of the data to obtain a single set of rate constants accounting for all the data. Analysis of the single-turnover kinetics provided measurements of equilibrium dissociation constants for 25/36-mer, dTTP, and PP_i equal to 18 nM (k_{off}/k_{on}), 18 μM (k_{-1}/k_1), and 2 mM (k_5/k_{-5}), respectively. The rate-limiting step during single-nucleotide incorporation has been identified as a conformational change, $E{\cdot}D_n{\cdot}N \rightarrow E'{\cdot}D_n{\cdot}N$, which occurs at a rate of 300 s^{-1} (k_2) upon binding of the correct dNTP. Accordingly, tighter binding of the transition states for the reaction resulting from the conformational change facilitates the phosphodiester bond formation. The chemical step itself was excluded as the rate-limiting step because of the small phosphothioate elemental effect. An observed rate constant of 70 s^{-1} for dTTP(αS) incorporation suggest that the chemical step (k_3) occurs at a fast rate, $\geq$9000 s^{-1}. Following chemistry, the resulting ternary complex, $E'{\cdot}D_{n+1}{\cdot}P$, undergoes a second conformational change at a rate of 1200 s^{-1} (k_4), leading to release of PP_i and translocation of the DNA to continue subsequent cycles of polymerization. The rate constants of the reverse steps, 100 s^{-1} (k_{-2}), $\geq$18 000 s^{-1} (k_{-3}) and 18 s^{-1} (k_{-4}), were derived as fits to the data based upon simulation of single-turnover kinetics of pyrophosphorolysis including measurements of pyrophosphate exchange and the overall equilibrium constant of 1.0×10^4 for elongation of E·25/36-mer to E·26/36-mer and analysis of the kinetics of the pulse–chase experiment. These studies provide the first complete and self-consistent thermodynamic descriptions of DNA polymerase and establish the basis for quantitative assessment of the reactions contributing to its extraordinary fidelity. The rate constants of the reverse reaction (pyrophosphorolysis) could only be measured by using an exonuclease-deficient mutant of gene 5 protein because of the high exonuclease activity of the wild-type enzyme. The double mutation D5A,E7A resulted in complete inactivation of the exonuclease activity. The mutant was fully characterized, and all rate constants for the polymerization reaction were shown to be identical with those of the wild-type enzyme. Its excision rate for single-stranded DNA was shown to be reduced by a factor of 10^6, while its excision rate for double-stranded DNA was not measurable.

DNA polymerases catalyze the rapid incorporation of dNMPs[1] while maintaining a remarkable substrate specificity, which has to change during each cycle of nucleotide addition as dictated by the sequence of the template DNA. The high fidelity of DNA replication is due to at least two distinct enzymatic reactions, the first involving selective incorporation of the correctly base-paired nucleotide and the second involving selective removal of mismatched bases by the proofreading 3′–5′ exonuclease (Kornberg 1980, 1982; Loeb & Kunkel, 1982). Previous characterization of DNA polymerization in the steady state has demonstrated the existence and importance of these reactions to fidelity but has not illuminated the mechanistic basis for selectivity in each step. Numerous models have been put forth to explain the extraordinary fidelity of DNA polymerization (Hopfield, 1974; Ninio, 1975; Loeb & Kunkel, 1982). Steady-state kinetic analysis of dNMP incorporation for correct and incorrect nucleotides has served to define specificity in terms of k_{cat}/K_m, but resolution of the contributions of K_m versus k_{cat} toward discrimination (Boosalis et al., 1987; Fersht, 1985) provide no mechanistic information with which to distinguish the various models for polymerization. Moreover, the mechanism by which the 3′–5′ exonuclease selectively removes mismatches has not been established other than to show a competition between the next correct nucleotide incorporation versus removal of the mismatch, although it has

† This work was supported by the Paul Berg Professorship from Penn State University (K.A.J.) and by NIH Postdoctoral Fellowship GM13135 (S.S.P.).

* Author to whom correspondence should be addressed.

[1] Abbreviations: dNMP, deoxynucleoside 5′-monophosphate; dNTP, deoxynucleoside 5′-triphosphate; dTTP, thymidine 5′-triphosphate; dTTP(αS), thymidine 5′-*O*-(3-α-thiotriphosphate); Tris, tris(hydroxymethyl)aminomethane; DTT, dithiothreitol; Pol I, *Escherichia coli* DNA polymerase I.

0006-2960/91/0430-511$02.50/0

been suggested that the selectivity may be a function of the fraying of the 3′-end of the duplex DNA. In addition, studies on the effect of pyrophosphate on fidelity have led to the suggestion of additional error correction mechanisms (Kunkel et al., 1986).

The kinetic and thermodynamic bases for the high fidelity of DNA replication can only be established by direct measurement of elementary steps in the DNA polymerase reaction. Recent application of transient kinetic methods to studies on Pol I Klenow fragment have provided the initial measurement of the contributions of individual reaction steps toward fidelity (Kuchta et al., 1987, 1988). However, these studies revealed two unusual and apparently anomalous properties of Pol I Klenow. First, it was shown that the binding of the incorrect and correct dNTPs occurs with nearly equal affinity. Second, the contribution of the exonuclease to fidelity was negligible, with the fastest reaction following misincorporation being the dissociation of the enzyme–DNA complex. Moreover, because these studies were performed on a variety of DNA templates and there are subtle differences in kinetic constants as a function of DNA sequence, it was not possible to provide a single kinetically and thermodynamically complete model to account for all of the data.

In order to test the generality of the conclusions derived by studies on Pol I and to examine which properties reflect the role of Pol I as an enzyme involved principally in repair rather than replication, we have chosen to examine a simple enzyme system responsible for replication of DNA, the T7 DNA polymerase. A complex of three proteins is sufficient to replicate the phage T7 DNA: T7 RNA polymerase, T7 DNA polymerase (gene 5 protein plus thioredoxin), and the helicase–primase (gene 4 protein) (Fuller & Richardson, 1985a,b; Richardson et al., 1987). The simplicity of the T7 replication system makes it an attractive model to examine in depth the complex mechanisms of DNA replication.

T7 DNA polymerase, the topic of these studies, is a heterodimer consisting of the phage T7 gene 5 protein (80 000 MW) and the host *Escherichia coli* thioredoxin protein (12 000 MW) (Modrich & Richardson, 1975). The two proteins form a 1:1 complex with an equilibrium dissociation constant of less than 5 nM; together they catalyze rapid and highly processive DNA polymerization. The gene 5 protein contains two activities, a 5′–3′ polymerization activity and a 3′–5′ exonuclease activity; the exonuclease active site resides near the amino terminus and the polymerase active site toward the carboxyl terminus. Thioredoxin by itself has no catalytic activity on the DNA. Its role has been thought to be merely structural, analogous to other accessory proteins of DNA polymerases. The increase in the DNA binding affinity of the gene 5 protein in presence of thioredoxin transforms it from a distributive to a highly processive enzyme (Tabor et al., 1987).

We present, in a series of three papers, the complete mechanism by which T7 DNA polymerase catalyzes the very fast and processive DNA synthesis with a high replication fidelity. The first paper describes the kinetics and thermodynamics of correct nucleotide incorporation and provides the basis for understanding replication fidelity and processive DNA synthesis. In addition, it describes the preparation and complete characterization of an exo$^-$ mutant of T7 DNA polymerase. The second paper describes the kinetics of misincorporation and presents quantitative data to support an induced-fit mechanism by which a correct nucleotide is selectively incorporated to the exclusion of incorrect nucleotides (Wong et al., 1991). In the last paper, we describe the kinetics of reaction at the exonuclease site and present a model for the partitioning of DNA between polymerase and exonuclease sites to define the error correction mechanism by the 3′–5′ exonuclease (Donlin et al., 1991). These three papers provide the first complete understanding of the reactions responsible for the high fidelity of DNA replication.

Materials and Methods

Enzymes. Wild-type gene 5 protein was purified by a reported procedure (Tabor et al., 1987) from *E. coli* BH215/pRS101 (Reutimann et al., 1985) provided by Arne Holmgren (Karolinska Institute, Stockholm, Sweden) and was greater than 95% pure by silver-stained SDS gel. The exo$^-$ gene 5 protein was purified from *E. coli* A179/pGA1-14/pGp1, the construction and purification of which is described elsewhere in this section. Thioredoxin was purified from an overproducing strain, *E. coli* SK3981/pBJK8, provided by B. Schuster (The Pennsylvania State University; Lunn et al., 1984). Purified Klenow fragment (KF) was provided by R. Kuchta and C. Catalano (The Pennsylvania State University). T4 polynucleotide kinase was purchased from New England Biolabs. Nucleoside diphosphate kinase was purchased from Sigma. T7 DNA polymerase described in this paper is a reconstituted complex of gene 5 protein (wild type) and thioredoxin incubated in a molar ratio of 1:20; the two proteins form a 1:1 complex (shown by using a gel-filtration column), and thioredoxin was added in excess to assure greater than 99% complexation of the gene 5 protein. Exo$^-$ T7 DNA polymerase was prepared similarly from the exo$^-$ mutant of gene 5 protein and will be specified whenever it is used.

Bacterial Strains, Plasmids, and Phage. *E. coli* A179 (Hfr-C(λ)*trxA*::*kan*) and plasmids pGP5-3 and pGP1-3 were obtained from S. Tabor and C. C. Richardson (Harvard Medical School; Tabor & Richardson, 1987). Plasmids pMa and pMc were gifts from H.-J. Fritz (Max-Planck-Institut für Biochemie). Helper phage M13K07 was obtained from R. Wagner (The Pennsylvania State University). *E. coli* strain MM294 was used for maintaining and propagating all plasmids. Strain JM101 was used for propagating single-stranded phages. Strain BMH 71-18 *mutS* was used for the primary transformation with mutagenized vectors. Strain W 71-18 was used for the second transformation to segregate wild-type and mutant plasmids. Plasmids pSPT18 and pSPT19, used for generating radiolabeled RNA probes, were obtained from Boehringer Mannheim.

Single-Stranded DNA–Cellulose (ssDNA–Cellulose). Denatured calf thymus DNA was cross-linked to microcrystalline cellulose (Sigma) by ultraviolet irradiation as described in Litman (1968).

Nucleotide Triphosphates and Other Materials. All four dNTPs were purchased from Pharmacia, and dTDP was purchased from Sigma. [α-^{32}P]dNTPs, [γ-^{32}P]ATP, dTTP-(αS), and [α-^{35}S]dTTP were purchased from New England Nuclear Labs, and their purity was estimated routinely by using PEI-cellulose (EM Science) thin-layer chromatography (PEI-cellulose TLC). Bio-Spin-30 columns were from Bio-Rad Labs, and the DE81 filters (2.5 cm) were from Whatman.

Synthetic Oligonucleotides. The oligonucleotides listed in Table I were synthesized on an Applied Biosystems 380A DNA synthesizer (DNA synthesis facility, The Pennsylvania State University) and purified by denaturing polyacrylamide gel electrophoresis (20% acrylamide, 8 M urea). The duplex primer/template, 25/36-mer, was formed by annealing approximately equimolar amounts of pure 25-mer and 36-mer at room temperature and purifying the duplex from the excess single-stranded oligonucleotides by nondenaturing poly-

Table I: Oligonucleotides

25/36-mer	GCCTCGCAGCCGTCCAACCAACTCA CGGAGCGTCGGCAGGTTGGTTGAGTAGGTCTTGTTT
30/60-mer	GCCTCGCAGCCGTCCAACCAACTCTACCCT CGGAGCGTCGGCAGGTTGGTTGAGATGGGATGGGATTGAAGTAGGTACACCAGTCGTTTA

acrylamide gel electrophoresis (20%). Concentrations of the oligonucleotides were estimated by UV absorbance at 260 nm with the following calculated extinction coefficients: 25-mer, $\epsilon = 249040$; 36-mer, $\epsilon = 377000$; 30-mer, $\epsilon = 302190$; 60-mer, $\epsilon = 668240$. Concentrations of the primer/templates, 25/36-mer and 30/60-mer, were obtained by incorporating single [α-^{32}P]dTMP and [α-^{32}P]dAMP in the respective DNA primer/templates by using KF or exo$^-$ T7 DNA polymerase and quantitating the incorporated nucleotides by filter binding assay.

Buffers. All experiments using T7 DNA polymerase were carried out in a buffer containing 40 mM Tris (pH 7.5), 1 mM EDTA, 1 mM DTT, 0.1 mg/mL BSA, and 50 mM NaCl. Buffers with magnesium contained in addition 12.5 mM $MgCl_2$. All experiments were carried out at 20 °C.

Mutagenesis of Gene 5 Protein. The double mutant D5A,E7A of gene 5 protein was prepared by using a synthetic oligonucleotide by the gapped-duplex method of Stannsens et al. (1989).

Overexpression and Purification. (A) Induction. E. coli A179/pGp1/pGA1-14 cells expressing the exo$^-$ mutant of T7 gene 5 protein were grown to an optical density of 0.4–0.6. We have found this to yield maximum expression of protein. Induction was done by rapidly increasing the temperature to 42 °C for 30 min followed by 4 h at 39 °C.

(B) Rapid Purification of Protein. Harvested cells were washed in rinse buffer (50 mM Tris·HCl, pH 8.1, 25 mM EDTA, 1.0 mM β-mercaptoethanol, 0.1 mM DTT, and 150 mM NaCl), repelleted, and weighed. Cells were resuspended in lysis buffer (same as rinse buffer but with 2.5 mM EDTA). Lysozyme was added to 0.3 mg/mL. After the solution was stirred at room temperature for 15 min, 4% sodium deoxycholate was added to a final concentration of 0.1%. Following lysis, 5 M NaCl was added to achieve a final concentration of 0.5 M and the lysate stirred on ice for an additional 15 min. The lysate was cleared by centrifugation at 39000*g* in a Sorvall SS-34 rotor at 18000 rpm for 15 min. The pellet was reextracted with a small volume of lysis buffer containing 0.1% sodium deoxycholate and 0.5 M NaCl and recentrifuged. The pooled supernatants were dialyzed against 6 L of buffer containing 10% glycerol and no salt in Spectra Por 7 dialysis tubing with a molecular weight cutoff of 25000. The protein was precipitated by the addition of 5% poly(ethylenimine) (PEI), pH 8, at 4 °C, to a final concentration of 0.3%. The precipitated protein was collected by centrifugation and extracted twice in a small volume of PEI extraction buffer (50 mM Tris-HCl, 2.5 mM EDTA, 1.0 mM β-mercaptoethanol, 0.1 mM DTT, and 500 mM NaCl). The protein was further purified and residual PEI removed by a 35%–70% ammonium sulfate cut. The precipitant was redissolved in buffer containing 50 mM KCl and 10% glycerol and dialyzed for no more than 4 h against 6 L of the same buffer, using 50000 molecular weight cutoff dialysis tubing. The dialyzed protein was loaded and washed onto a column of ssDNA–cellulose (24 cm × 2.5 cm, 120 mL bed volume, 66 mL void volume), and a linear gradient of 100–350 mM NaCl was immediately started. The polymerase was eluted between 170 and 200 mM NaCl. Peak fractions were concentrated and then dialyzed against buffer containing 50% glycerol and stored at −80 °C.

The above protocol for purification of the exo$^-$ gene 5 protein was adapted from the procedure reported for the overexpressed T4 DNA polymerase (Lin et al., 1987). The method differs from the protocol for gene 5 protein purification reported in the literature (Tabor & Richardson, 1987). Our modified protocol is now the method of choice for the wild-type and the exo$^-$ gene 5 proteins. We have retained the EDTA rinse step in order to exclude the possibility of iron-induced inactivation of the exonuclease activity. We have, however, switched to a detergent (sodium deoxycholate) lysis rather than freeze–thaw, partly in consideration of time but mostly because we felt that the detergent lysis was more efficient. We have retained the addition of 500 mM NaCl to aid the recovery of the overproduced protein in the supernatant. Tabor and Richardson observed that without addition of the additional salt the overproduced protein is insoluble. We feel that the overproduced protein is probably not so much insoluble but instead is tightly bound to the DNA precipitated in the pellet. The addition of NaCl thus serves to disupt any protein–DNA interactions and thereby improves the recovery of protein in the supernatant. Typically ≥90% of the protein is recovered under our lysis conditions. For the two dialysis steps, high molecular weight cutoff membranes must be used for two reasons. First, a low molecular weight contaminant is not efficiently removed in the chromatographic steps but can be dialyzed away. Second, the speed of the dialysis is critical because we have found that dialysis into low-salt buffer (≤100 mM NaCl), which was necessary for the PEI step as well as for the ssDNA–cellulose step, often resulted in precipitated protein if the dialysis proceeded for longer than 4 h. With this shortened protocol, the entire purification process from lysis onward can be accomplished in 24 h and requires only one column. The resultant protein is judged to be ≥99% pure on a silver-stained SDS–polyacrylamide gel. In particular, protein purified by this method is free of the copurifying proteolytic fragments found in both of the reported procedures (Tabor et al., 1987; Reutimann et al., 1985) in the literature.

Reconstitution of T7 DNA Polymerase. T7 DNA polymerase was routinely reconstituted only prior to the experiment by the following procedure. Fresh DTT (0.5 M) was added to a solution of thioredoxin to a final DTT concentration of 5 mM. (Thioredoxin has to be in the reduced form in order to form an active complex with the gene 5 protein.) Gene 5 protein was then added to the reduced thioredoxin such that the molar ratio of gene 5 protein to thioredoxin was 1:20.

5′ ^{32}P Labeling of 25/36-mer. Primer/template, 25/36-mer, was 5′-radiolabeled with T4 polynucleotide kinase by using the procedure described in Maniatis et al. (1982) for 5′-labeling of blunt-ended duplex DNA. The reaction was quenched with 0.1 M EDTA, followed by purification with a Bio-Spin-30 column, which removed the contaminating nucleotides from the labeled DNA primer/template.

3′ [^{32}P]dTMP Labeling of 25/36-mer. 25/36-mer (1.0 μM) was added to a mixture of dTTP (10 μM), [α-^{32}P]dTTP (10000–50000 counts/pmol), and T7 DNA polymerase (exo$^-$, 50 nM) in magnesium buffer. The reaction was incubated at room temperature for 30 min and quenched with 0.1 M

EDTA. The solution was extracted once with phenol–chloroform and the unincorporated nucleotides were removed by using a series of two Bio-Spin-30 columns.

Synthesis of [γ-^{32}P]dTTP. [γ-^{32}P]dTTP was prepared by an exchange reaction between [γ-^{32}P]ATP and dTDP catalyzed by the enzyme nucleoside diphosphate kinase (NDPK) as follows. NDPK (10 units) was added to a mixture of [γ-^{32}P]ATP (100 μL, 3.0 μM) and dTDP (20 μM) in Tris–Mg^{2+} buffer (50 mM Tris and 10 mM $MgCl_2$). The reaction was incubated at room temperature for 5 min and quenched with 0.1 M EDTA. The reaction solution was spotted on a PEI-cellulose TLC plate and developed with 0.3 M potassium phosphate buffer (pH 7.0) to resolve the nucleotides. The PEI-cellulose containing the [γ-^{32}P]dTTP band was scraped and extracted 5 times with 0.5-mL aliquots of 1.0 M triethylammonium bicarbonate buffer (TEAB, pH 7.0). The fractions were pooled and evaporated to dryness under vacuum. [γ-^{32}P]dTTP was further purified on a DEAE Sephadex-A25 column eluted with a 0.1–1 M TEAB gradient. The purity of the compound was checked before use by PEI-cellulose TLC.

^{32}P-Labeled Calf Thymus DNA. Single-stranded calf thymus DNA (2 mg/mL) was incubated with T4 DNA polymerase (500 nM) in the presence of 300 μM of each dNTP at a specific activity of 50 Ci/mmol for 15 min at room temperature under standard reaction buffer conditions. Reaction was quenched by addition of EDTA to a final concentration of 100 mM. Proteins were removed by two sequential phenol–chloroform extractions. Unincorporated dNTPs were removed by centrifugation through Bio-Spin-30 centrifuge desalting columns.

Measurement of the Dissociation Rate Constant of 25/36-mer. The dissociation rate of 25/36-mer from T7 DNA polymerase was measured as follows. 5′-Labeled 25/36-mer (200 nM) was preincubated with T7 DNA polymerase (100 nM) in the absence of magnesium. Calf thymus DNA (1 mg/mL, enzyme trap) was added to the above complex and incubated for time intervals ranging from 5 to 60 s. At the end of the period, Mg^{2+}·dTTP (50 μM) was added and the reaction was stopped with 0.1 M EDTA after a constant interval of 10 s. The amount of 26/36-mer formed was analyzed by sequencing gel electrophoresis. The data followed a single exponential at a rate of 0.2 s^{-1}, representing the rate constant for dissociation of the 25/36-mer from the polymerase.

Rapid-Quench Experiments. Rapid-quench experiments were carried out in an apparatus designed and built by Johnson (1986). Typically, the experiments were carried out by loading the enzyme in one loop (45 μL) and substrate in the second loop (45 μL) of tubing. The reactions were started by rapidly mixing the two reactants and then quenching with 0.3 M EDTA (final concentration) after time intervals ranging from 3 ms to several seconds.

The experiments measuring the K_ds of 25/36-mer and dTTP, the elemental effect of dTTP(αS), and the processivity studies were all carried out by loading a preincubated mixture of T7 DNA polymerase and DNA in one syringe and mixing it with dNTPs and Mg^{2+} from the second syringe. The products were analyzed by either filter binding assay, sequencing gel electrophoresis, or PEI-cellulose TLC, depending on the position of the radiolabel placed on the substrates. The pyrophosphorolysis experiments required incubation of inorganic pyrophosphate with E·DNA in an EDTA buffer because higher concentrations of PP_i (≥5 mM) precipitated after long times in the presence of magnesium. At pyrophosphate concentrations greater than 2 mM, the reactions contained the same amount of additional magnesium. We have observed no difference in the reaction kinetics whether PP_i was preincubated with E·DNA or dNTP.

Scheme I

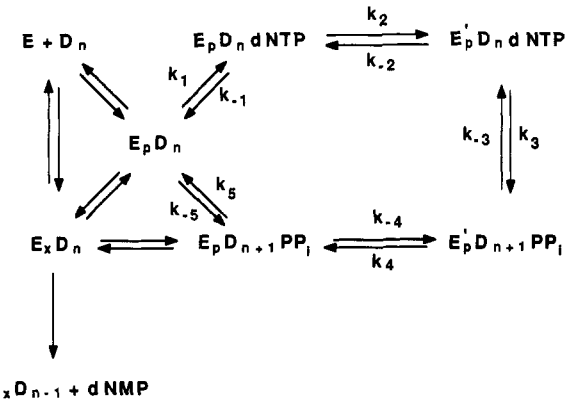

Product Analysis. Experiments carried out with [α-^{32}P]-dNTPs were analyzed by DE81 filter binding assays. The DE81 filters were washed with 0.3 M ammonium formate buffer (pH 8, adjusted with ammonium hydroxide). The radiolabeled DNA remained bound to the filter while the unincorporated dNTPs were washed out.

When 5′-labeled primer/templates were used as substrates, the products were resolved on a 15–18% sequencing gel and visualized by autoradiography. The product and the substrate DNAs were quantitated either by scanning the autoradiogram with a densitometer or by cutting the radioactive bands on the gel and counting on a scintillation counter or both.

PEI-cellulose TLC was used to resolve ^{32}P-labeled dTMP and dTTP, the respective products of the exonuclease and pyrophosphorolysis reactions during the pyrophosphorolysis experiments. The PEI-cellulose TLC plates were developed with 0.3 M potassium phosphate buffer (pH 7.0). Cold nucleotides were spotted along with the reaction mixture, which allowed the spots to be visualized by both autoradiography and UV light. The TLC plates were cut and counted on a liquid scintillation counter.

The pyrophosphate exchange experiments were analyzed for the formation of [^{32}P]pyrophosphate by using charcoal columns as described by Johnson (1983).

Exonuclease: Duplex DNA. ^{32}P-labeled calf thymus DNA (1 mg/mL) was incubated with up to 5 μM exo$^-$ or up to 0.1 μM wild-type polymerase in standard reaction conditions for 5 min. Reactions were quenched by the addition of EDTA to a final concentration of 100 mM. Exonuclease activity was quantitated by DE81 filter binding assay.

Exonuclease: Single-Stranded DNA. 5′-^{32}P-labeled 20-mer (50 nM) was mixed with enzyme (500 nM), and the products were monitored by excision and liquid scintillation counting of bands from a denaturing sequencing gel.

Exonuclease: Single-Mismatched DNA. 5′-^{32}P-labeled 25A/35-mer (50 nM) was mixed with enzyme (500 nM), and the products were monitored by excision and liquid scintillation counting of bands from a denaturing gel.

Data Analysis. The kinetic data were modeled by using the KINSIM kinetic simulation program provided by Carl Frieden and Bruce Barshop (Washington University, St. Louis, MO; Barshop et al., 1983) as modified by Anderson et al. (1988) and refined by regression analysis to obtain the best fit by using a modification of the program of Zimmerlie and Frieden (1989). All the curves were fitted to a single mechanism shown in Scheme I and rate constants shown in Table II. The K_d curves were fitted to a hyberbola or the quadratic equation

Table II: T7 DNA Polymerase Kinetic Constants[a]

reaction	k_+	k_-	K_{eq}
$E + D_n \rightleftharpoons E{\cdot}D_n$	11 μM^{-1} s^{-1}	0.2 s^{-1}	56 μM^{-1}
$E{\cdot}D_n$ + dTTP $\rightleftharpoons$ $E{\cdot}D_n{\cdot}dTTP$	>50 μM^{-1} s^{-1}	>1000 s^{-1}	0.054 μM^{-1}
$E{\cdot}D_n{\cdot}dNTP \rightleftharpoons E'{\cdot}D_n{\cdot}dNTP$	300 ± 30 s^{-1}	100 ± 3 s^{-1}	3.0
$E'{\cdot}D_n{\cdot}dNTP \rightleftharpoons E'{\cdot}D_{n+1}{\cdot}PP_i$	>9000 s^{-1}	>18000 s^{-1}	0.5
$E'{\cdot}D_{n+1}{\cdot}PP_i \rightleftharpoons E{\cdot}D_{n+1}{\cdot}PP_i$	1200 ± 280 s^{-1}	18 ± 0.5 s^{-1}	67
$E{\cdot}D_{n+1}{\cdot}PP_i \rightleftharpoons E{\cdot}D_{n+1}$ + PP_i	>1000 s^{-1}	>0.5 μM^{-1} s^{-1}	2 mM
$E{\cdot}D_n \rightarrow E{\cdot}D_{n-1}$ + dNMP	1.8 s^{-1}		

[a] These kinetic constants represent the best fit for all of the kinetic and equilibrium data given in this paper. Equilibrium constants and free energies were calculated for the forward reaction as written. The internal equilibrium constant is the product of $K_2K_3K_4$ = 100 and the overall equilibrium constant given by the product $K_1K_2K_3K_4K_5$ = 10000 for the forward reaction. Conditions: 40 mM Tris, 12 mM $MgCl_2$, 50 mM NaCl, 1 mM DTT, and 0.1 mg/mL BSA, pH 7.5 at 20 °C.

by nonlinear regression using RS 1 (BBN Software Products Corp., Cambridge, MA).

Results

In this paper, we present experiments leading to elucidation of the mechanism of single correct nucleotide addition. The pre-steady-state kinetic experiments were conducted with a rapid-quench instrument because of the very fast rate of DNA synthesis catalyzed by T7 DNA polymerase. It is important to note that we have found small differences (less than 10-fold) in the measured rates and equilibrium constants depending on the nucleotide added and the sequence of the neighboring bases. Thus, by taking care to perform all experiments with the same primer/template and nucleotide in both the forward and the reverse directions, we have established a single set of rate and equilibrium constants in a mechanism to quantitatively account for all of our data by a single, complete kinetic model shown in Scheme I with the rate constants summarized in Table II. This provides the basis to understand the kinetics of processive DNA synthesis catalyzed by T7 DNA polymerase.

All kinetic studies of T7 DNA polymerase were carried out with a synthetic primer/template of a predefined DNA sequence. Homopolymers, such as oligo(dT)–poly(dA), widely used as substrates for activity assays and for kinetic studies (Huber et al., 1987; Bryant et al., 1983), are in general unsuitable for quantitative studies of the polymerase. This is mostly due to the tendency of the short oligo(dT) primers to stack on the poly(dA) template, giving a heterogeneous mixture of primer/templates and preventing accurate determination of the 3′-end concentration, both of which preclude proper quantitation and interpretation of the results. Therefore, by using gel-purified synthetic primer/templates of predefined sequences, we were able to accurately measure the 3′-end concentration and the homogeneity of the primer/templates was also assured. Of the several small primer/templates tested, the oligomer 25/36-mer was found to have an optimum length of duplex DNA that permitted its tight binding to T7 DNA polymerase. Smaller primer/templates, for instance 9/20-mer and 13/20-mer, which have been used as substrates of the Klenow fragment of Pol I (Kuchta et al., 1987), proved too small, judged from their relatively weaker binding affinity for T7 DNA polymerase. The primer/template, 25/36-mer, used in this study has a random but

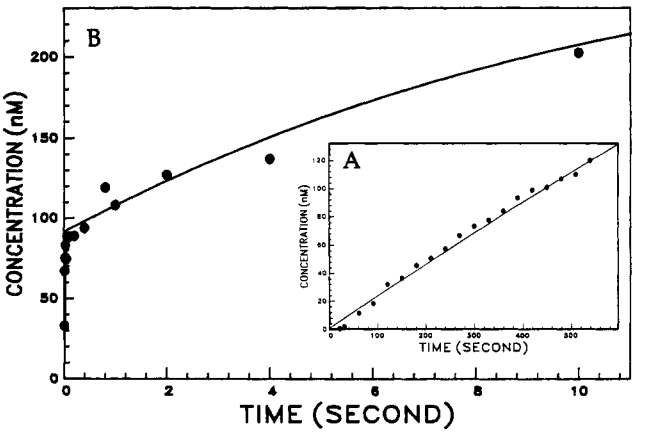

FIGURE 1: Steady-state and pre-steady-state kinetics of dTTP incorporation into 25/36-mer. (A) T7 DNA polymerase (1.0 nM) was added to 25/36-mer (1.0 μM) and $Mg^{2+}{\cdot}[\alpha$-$^{32}P]$dTTP (50 μM) to initiate the reaction. Polymerization was quenched with 0.3 M EDTA at time intervals ranging from 20 s to 10 min. The reaction products were analyzed by DE81 filter binding assay as described under Materials and Methods. The data (●) were fitted to a straight line with a slope equal to 0.24 s^{-1} per enzyme site, which represents the steady-state rate of dTTP incorporation into 25/36-mer. (B) A preincubated solution of T7 DNA polymerase (100 nM) and 25/36-mer (300 nM) was mixed with $Mg^{2+}{\cdot}[\alpha$-$^{32}P]$dTTP (30 μM) in a rapid-quench instrument. The reactions were quenched with 0.3 M EDTA, and the data (●) were obtained from the DE81 filter binding assay. The data fit to a biphasic curve with rate constants equal to 190 s^{-1} and 0.2 s^{-1}. The solid line was calculated by computer simulation to the mechanism shown in Scheme I with a 0.2 s^{-1} DNA dissociation rate.

predefined DNA sequence designed to enable single-nucleotide incorporation studies.

The extremely fast DNA polymerization reactions catalyzed by T7 DNA polymerase were conducted with the rapid-quench technique. The proper use of this approach necessitated a quench reagent that would stop the reactions rapidly. After testing several quench reagents, the two reagents 0.3 M EDTA and 0.5 M HCl (final concentrations) were found to be sufficient and equally efficient as quenchers and provided identical rate profiles. We have observed, however, that a lower concentration of EDTA, ≤0.2 M for instance, did not stop the reactions rapidly enough. Because of its practical convenience as a quench reagent, 0.3 M EDTA was used rather than HCl for the data shown in this paper.

Steady-State and Pre-Steady-State Polymerization Kinetics of dTTP Incorporation. The steady-state kinetics of 25/36-mer (Table I) elongating to 26/36-mer were measured by using a large excess of 25/36-mer (1 μM) over T7 DNA polymerase (1 nM) and by incorporating $[\alpha$-$^{32}P]$dTTP (50 μM). Figure 1A shows the time course of dTMP incorporation. The steady-state rate constant was calculated from the ratio of the slope divided by the enzyme concentration to give a value of 0.2 s^{-1}. This steady-state rate measures the slowest step during single-nucleotide incorporation and, as shown below, represents the slow dissociation of the product DNA, 26/36-mer, from the enzyme.

A pre-steady-state experiment was conducted under conditions where the DNA concentration was in 3-fold excess of the enzyme concentration in order to observe the kinetics of the first and subsequent turnovers of the enzyme. The reaction was carried out by mixing a solution containing the preincubated complex of T7 DNA polymerase (100 nM) and 25/36-mer (300 nM) with $Mg^{2+}{\cdot}[\alpha$-$^{32}P]$dTTP (30 μM). Polymerization was quenched with 0.3 M EDTA at time intervals ranging from 5 ms to 10 s. The resulting time course of $[^{32}P]$dTMP incorporation, shown in Figure 1B, follows biphasic

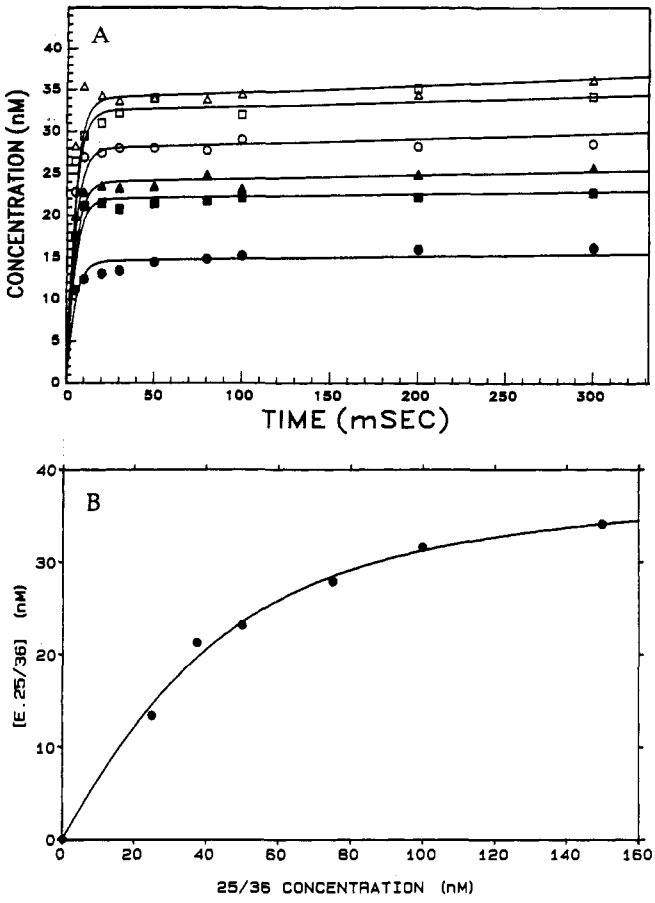

FIGURE 2: Active-site titration of T7 DNA polymerase with 25/36-mer. (A) A solution of T7 DNA polymerase (40 nM) preincubated with increasing concentrations of 5′-^{32}P-labeled 25/36-mer was mixed with a solution of Mg^{2+}·dTTP (100 μM) to start the reactions. The reactions were quenched with 0.3 M EDTA, and the products were quantitated by sequencing gel electrophoresis. 25/36-mer concentrations were as follows: (●), 25 nM; (■), 37.5 nM; (▲), 50 nM; (○), 75 nM; (□), 100 nM; and (△), 150 nM. The solid lines were obtained by computer simulation to the mechanism shown in Scheme I and an E·25/36-mer K_d equal to 18 nM. (B) The data (●) represent the plot of the burst amplitude determined from the above experiment versus the respective 25/36-mer concentrations. The solid line is the fit of the data to the quadratic equation $[E{\cdot}D] = 0.5(K_D + E_t + D_t) - [0.25(K_D + E_t + D_t)^2 - (E_tD_t)]^{1/2}$, which gave an E·25/36-mer K_d of 17.8 ± 2.0 nM.

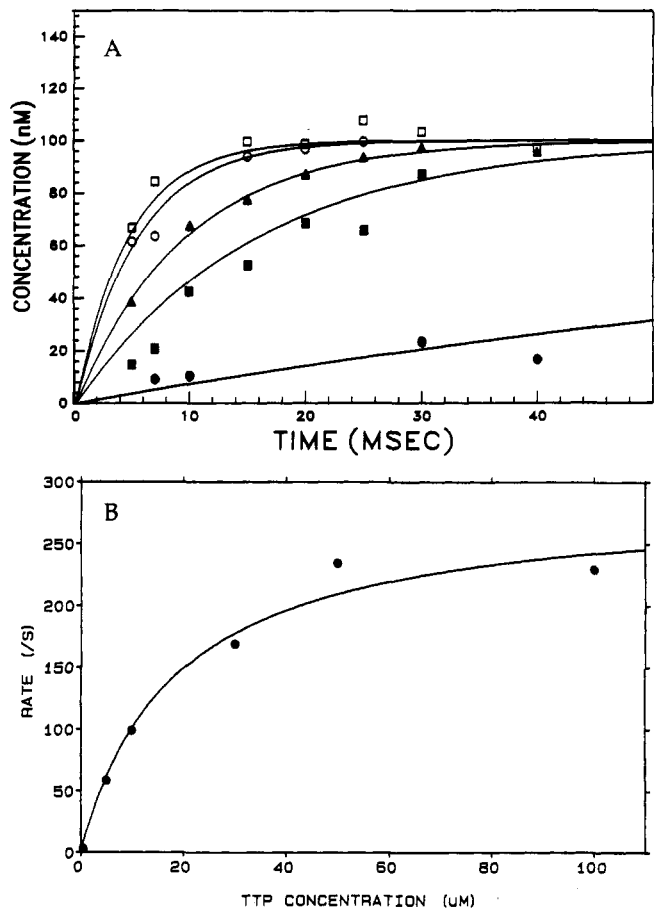

FIGURE 3: dTTP concentration dependence on the pre-steady-state burst rate. (A) A preincubated solution of T7 DNA polymerase (100 nM) and 5′-^{32}P-labeled 25/36-mer (200 nM) was mixed with increasing concentrations of Mg^{2+}·dTTP to start the reactions. dTMP incorporation was quantitated by sequencing gel assay. The dTTP concentrations were (●), 0.5 μM; (■), 5 μM; (▲), 10 μM; (○), 30 μM; and (□), 50 μM. The solid lines are curves simulated to the mechanism shown in Scheme I and rate constants shown in Table II. (B) The pre-steady-state rates obtained by fitting the data from the experiment described above were plotted against the dTTP concentrations. The rate data (●) were fitted to a hyperbola which gave the dTTP K_d of 18 ± 4 μM and a maximum incorporation rate equal to 287 ± 20 s^{-1}.

kinetics. The fast phase represents the first turnover, with a rate of 190 s^{-1} and an amplitude equal to 90% of the enzyme sites in this experiment. The subsequent turnovers occur at a slower rate of 0.2 s^{-1}, which is the same as the steady-state rate. The pre-steady-state burst observed in this experiment clearly indicates that the rate-limiting step during steady-state incorporation of a single correct nucleotide occurs after the chemical step. In fact, the rate-limiting step in this assay is the slow dissociation of the DNA from the enzyme, which was measured and confirmed independently as 0.2 s^{-1} by using a trap experiment, described under Materials and Methods (data not shown).

Active-Site Titration of E·DNA. The observed biphasic nature of the pre-steady-state rate profile during single-nucleotide incorporation suggests the presence of a stable E·DNA complex. Since catalysis was much faster than the equilibration of the enzyme and DNA (E + DNA ⇄ E·DNA), it was possible to titrate the enzyme active site with the DNA simply by examining the DNA concentration dependence of the pre-steady-state burst amplitude. The active-site titration experiment was carried out at a fixed enzyme concentration; T7 DNA polymerase (40 nM) was preincubated with increasing concentrations of 25/36-mer (25–250 nM) in the absence of magnesium (to prevent the exonuclease reaction). The E·25/36-mer complex present in the preincubation mixture was quantitated by reacting the mixture with the next correct nucleotide, dTTP, and measuring the time dependence of the formation of 26/36-mer. The resulting time courses of 26/36-mer formation at various DNA concentrations are shown in Figure 2A. It is clearly seen that the burst amplitudes increased as a function of increasing 25/36-mer concentration and reached a maximum close to the concentration of the enzyme in the reaction. The burst amplitude, when plotted against the 25/36-mer concentration (Figure 2B) and fitted to the quadratic equation, provided measurement of the true K_d for formation of a productive complex between 25/36-mer and T7 DNA polymerase equal to 17.8 ± 2 nM. With the knowledge that the dissociation rate constant (k_{off}) of 25/36-mer was 0.2 s^{-1}, the apparent second-order binding rate constant $k_{on} + k_{off}/K_d = 1.12 \times 10^7$ M^{-1} s^{-1} was thus calculated.

Measurement of K_d of dTTP. The equilibrium dissociation constant of dTTP was determined by measuring the rate of the E·25/36-mer → E·26/36-mer reaction, carried out at a fixed E·25/36-mer concentration (100:200 nM) and varying

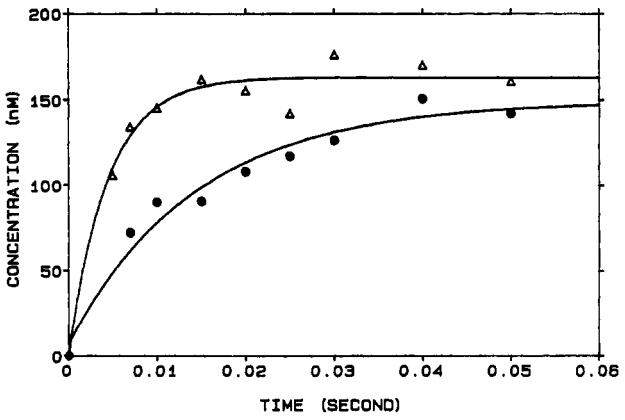

FIGURE 4: dTTP(αS) elemental effect on the pre-steady-state burst rate. A solution of T7 DNA polymerase (100 nM) was preincubated with 25/36-mer (200 nM) and mixed with Mg^{2+}·[α-^{32}P]dTTP (50 μM) and Mg^{2+}·[α-^{35}S]dTTP (50 μM) to initiate the parallel reactions. The products were quantitated by DE81 filter binding assay. The curve (Δ) is the pre-steady-state time course of dTMP incorporation fitted to a first-order rate of 220 s^{-1}. The curve ($\bullet$) is the pre-steady-state time course of dTTP(αS) incorporation fitted to a rate of 70 s^{-1}. The elemental effect of 3.1 was determined from the ratio of the measured pre-steady-state rates.

dTTP concentrations (0.5–100 μM). As shown in Figure 3A, the single-turnover rates of nucleotide incorporation increased with increasing concentrations of dTTP, and when the rates were plotted against the dTTP concentrations, the data fit a hyperbola supporting the pathway

$$E{\cdot}D_n + dTTP \overset{K_d}{\rightleftharpoons} E{\cdot}D_n{\cdot}dTTP \xrightarrow{k_p} E{\cdot}D_{n+1}{\cdot}PP_i$$

$$k_{obs} = \frac{k_p[dTTP]}{[dTTP] + K_d} \qquad (1)$$

where K_d represents the equilibrium dissociation constant of dTTP and k_p is the maximum rate of 26/36-mer formation. The hyberbolic plot (Figure 3B) gave a dTTP K_d of 18 ± 4 μM and the maximum rate (k_p) of single nucleotide incorporation equal to 287 ± 20 s^{-1} at 20 °C. Preliminary stopped-flow experiments (data not shown) measuring dTTP binding facilitated by a protein fluorescence change upon dNTP binding indicated a fast binding rate of dTTP, ≥5 × 10^7 M^{-1} s^{-1}. Hence, from the measured K_d of dTTP, we place a lower limit on the dissociation rate constant of dTTP from E·D_n to be ≥1000 s^{-1}.

Rate-Limiting Step during Processive Polymerization. The next obvious question is whether the observed rate of 300 s^{-1} is a direct measure of the rate of phosphodiester bond formation. It has been shown that a rate-limiting chemical step involving making or breaking of a phosphate bond shows a phosphothioate elemental effect (Benkovic & Schray, 1971). Therefore, if the α phosphate of dNTP is replaced with the phosphothioate group, the single-turnover rate should decrease around 100-fold if the observed rate is a direct function of the chemical step (Mizrahi et al., 1985). The phosphothioate analogue of the nucleotide, dTTP(αS), was used to measure the elemental effect. The resulting single-turnover rate of dTTP(αS) incorporation, 70 s^{-1}, when compared with the dTTP incorporation rate, 220 s^{-1}, measured at 50 μM dNTP concentrations (Figure 4), provided an elemental effect of 220/70 = 3.1. This elemental effect is very small, indicating that the chemical step is not the rate-limiting step. Furthermore, on the basis of the observed rate of 70 s^{-1} with dTTP(αS) and by using a lower limit of the expected elemental effect equal to 60, the highest elemental effect we have observed (Wong et al., 1991), the rate of the chemical step can be calculated from eq 2 [for derivation, refer to the appendix section of the following paper in this issue (Wong et al., 1991)] as ≥9000 s^{-1} (k_2) for incorporation of dNTP and a rate ≥60 times slower for the thio analogue of dNTP.

$$k_2 = k_f \Lambda_1 \frac{\sigma - 1}{E_{obs} - 1}$$

$$\Lambda_1 = \frac{K_1 + 1}{K_1} \qquad (2)$$

k_2 is the rate of the chemical step, σ is the maximum elemental effect, E_{obs} is the observed elemental effect, k_f is the net forward rate of 300 s^{-1}, and K_1 is defined as k_1/k_{-1}.

On the basis of the results from the above experiments, we suggest that the 300 s^{-1} rate-limiting step is a conformational change that occurs following the binding of the correct dNTP and preceding the very fast chemical step. Additional data, presented in the accompanying paper (Wong et al., 1991), demonstrate the role of such a conformational change in proper recognition of the correct dNTP by an "induced-fit" type of mechanism.

Kinetics of the Reverse Polymerization Reaction. Since the rate-limiting step in dNMP incorporation occurs before chemistry, it is not possible to extract any more mechanistic information about the remaining steps, such as the chemical step and the PP_i release step, from kinetic studies of the forward polymerization reaction. Therefore, it is necessary to examine the kinetics of the reverse reaction, pyrophosphorolysis, in order to delineate the complete mechanism.

Pyrophosphorolysis is the exact reverse of the dNTP incorporation reaction; the reaction of PP_i with the 3′-base of E·D_{n+1} results in pyrophosphorolysis to form dNTP and E·D_n. Under the experimental conditions used to measure the reverse reaction, the absence of the next correct dNTP, the very high 3′–5′ exonuclease activity of T7 DNA polymerase competes with the pyrophosphorolysis reaction and results in hydrolysis of the 3′-base of E·D_{n+1} to form dNMP and E·D_n:

$$\begin{array}{ccc} E{\cdot}D_{n+1} & \xrightarrow[k_{PP_i}]{PP_i} & E{\cdot}D_n + dNTP \\ H_2O \downarrow k_x & & \\ E{\cdot}D_n + dNMP & & \end{array}$$

The single-turnover time courses of the parallel exonuclease and the pyrophosphorolysis reactions were measured by using a 3′-[^{32}P]dTMP-labeled 26/36-mer as the DNA substrate. The experiment was carried out with a 2-fold excess of enzyme over DNA. T7 DNA polymerase (500 nM), 26/36-mer (250 nM), and PP_i (10 mM) were preincubated in one syringe in the absence of magnesium, and the reaction was initiated by adding Mg^{2+}·dTTP (20 μM) from the second syringe (the cold nucleotide, dTTP, was added to trap the radiolabeled dTTP formed by the pyrophosphorolysis reaction). The reaction was quenched with 0.3 M EDTA, and the substrate, 26/36-mer, and the products, dTTP and dTMP, were resolved by PEI-cellulose TLC and quantitated by liquid scintillation counting. Shown in Figure 5, the resulting time courses illustrate partitioning of the 3′-base of the 26/36-mer by the exonuclease and the pyrophosphorolysis reactions to form both dTTP and dTMP at an apparent rate of 2.5 s^{-1} for each reaction. Since the exonuclease reaction of 1.8 s^{-1} (measured in the absence of PP_i) competes effectively with pyrophosphorolysis, the data indicate that the rate of the reverse reaction must be comparable. This slow rate of the reverse reaction could be a function of a highly unfavorable equilibrium constant of the

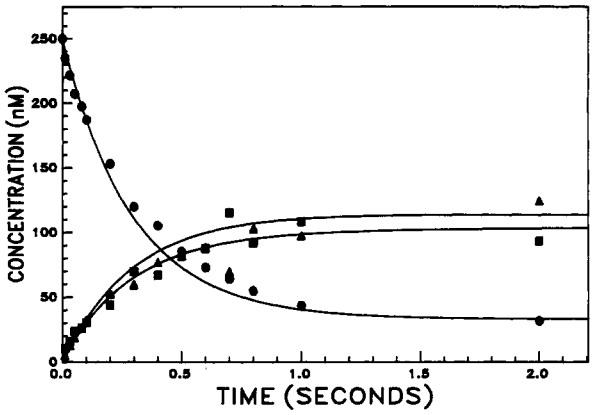

FIGURE 5: Single-turnover pyrophosphorolysis and exonuclease kinetics. A preincubated mixture of T7 DNA polymerase (500 nM), 3′-[^{32}P]dTMP-labeled 26/36-mer (250 nM), and PP_i (10 mM) was mixed with Mg^{2+}·dTTP (25 μM) to start the reaction. The reactions were quenched with 0.3 M EDTA, and the products were resolved by PEI-cellulose chromatography as described under Materials and Methods. Curve (●) represents the time course of disappearance of 26/36-mer, curve (▲) represents formation of [^{32}P]dTMP, the exonuclease product, and (■) represents formation of [^{32}P]dTTP, the pyrophosphorolysis product. The solid lines were calculated by simulation to the mechanism shown in Scheme I and rate constants in Table II.

Table III: Comparison of Wild-Type and Exo$^-$ T7 Polymerase

parameter	T7 wild type	T7 exo$^-$
$K^{pol}_{d,DNA}$ (nM)	23 ± 9	16 ± 1
$K_{d,dNTP}$ (μM)	18 ± 4	21 ± 2
k_{pol} (s^{-1})	287 ± 20	242 ± 12
K_{d,PP_i} (mM)	2.0 ± 0.24	2.0 ± 0.22
k_{PP_i} (s^{-1})		1.0 ± 0.02
$K^{exo}_{m,DNA}$ (nM)	690 ± 240	800 ± 100
k_{exo} (s^{-1})	105 ± 8	(6.9 ± 0.5) × 10^{-4}

reverse reaction or a function of a slow step before chemistry, which limits the rate of the reverse reaction. However, detailed analysis of the pyrophosphorolysis reaction was not possible because the kinetics were dominated by the exonuclease reaction. Further investigation of the reverse reaction, in the absence of the complicating exonuclease reaction, was therefore necessary and it became possible only after an exo$^-$ mutant of T7 DNA polymerase was prepared. The preparation of the exo$^-$ mutant by site-directed mutagenesis is described under Materials and Methods. Also documented in Table III is the unaltered polymerase activity of the mutant but an impressive 6 order of magnitude decrease in the exonuclease rate.

Pyrophosphorolysis Reaction Catalyzed by the Exo$^-$ Mutant of T7 DNA Polymerase. By using the exo$^-$ mutant of T7 DNA polymerase, we were able to examine the kinetics of the reverse reaction in greater detail. Figure 6A shows the kinetics of a single turnover of the pyrophosphorolysis reaction obtained at 10 mM PP_i. The PP_i concentration dependence of the single-turnover rate fit a hyperbola with a maximum velocity of 1.0 ± 0.02 s^{-1} and a dissociation constant for PP_i binding of 2.0 ± 0.22 mM (Figure 6B). Note that the single-turnover time course of the pyrophosphorolysis reaction, shown in Figure 6A, is a complex function of all reverse rates and equilibrium constants and hence was analyzed by computer simulation of the complete reaction scheme including data defining the overall equilibrium constant (see below) to derive the rate constants shown in Table II. The slow single-exponential rate of pyrophosphorolysis could only be interpreted by the presence of an additional step in the pathway between PP_i binding and chemistry; otherwise, the pyrophosphorolysis kinetics would be biphasic if the chemical step

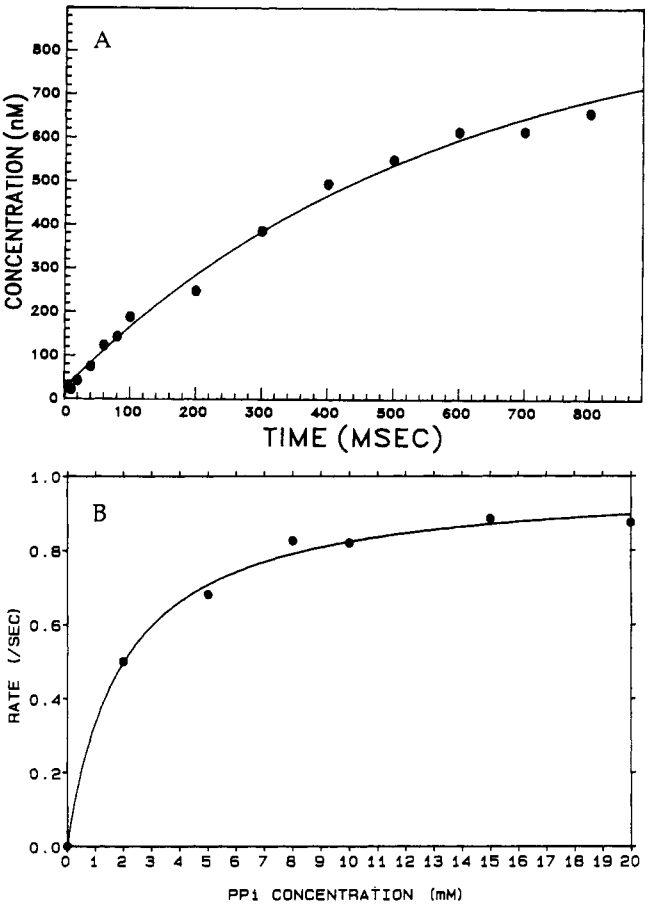

FIGURE 6: Single-turnover pyrophosphorolysis kinetics of the exo$^-$ mutant of T7 DNA polymerase and determination of the K_d of PP_i. (A) A solution of T7 DNA polymerase (exo$^-$, 2.0 μM) and Mg^{2+}·3′-[^{32}P]dTMP-labeled 26/36-mer (1.0 μM) was mixed with a solution of dTTP (20 μM) and PP_i (10 mM) to start the reaction. The time course of [^{32}P]dTTP formation (●) was computer simulated to the mechanism shown in Scheme I and rate constants shown in Table II. (B) A solution of T7 DNA polymerase (800 nM) and 3′-[^{32}P]-dTMP-labeled 26/36-mer (400 nM) was mixed with increasing concentrations of PP_i (2.0–20 mM) and dTTP (20 μM), and the pyrophosphorolysis rates were determined by quantitating the formation of [^{32}P]TTP. The data (●) were fitted to a hyperbola, which gave a K_d of 2.0 ± 0.22 mM for PP_i binding and a maximum pyrophosphorolysis rate equal to 1.0 ± 0.02 s^{-1}.

Table IV: Pyrophosphorolysis Rates[a]

3′ base sequence	TC* AG	CA* GT	TA* AT	CC* GG	GT* CA	AA* TT	AT* TA
rate (s^{-1}) (5 mM PP_i)	0.05	0.16	0.17	0.2	0.22	0.3	0.7

[a] An asterisk indicates the base being removed by pyrophosphorolysis.

occurred immediately after PP_i binding. Computer simulation of the data from this experiment and the previous experiment has allowed us to estimate the rate of this step as 18 s^{-1} (k_{-4}) and 1200 s^{-1} (k_4). We have assigned this step to a second conformational change of the enzyme occurring before the reverse chemical reaction. The pyrophosphorolysis reaction rate was found to be highly sensitive to the 3′-base being removed and to the penultimate base pair of the primer/template, as shown in Table IV. The reaction rate at 5 mM PP_i varied over a range of 0.05–0.7 s^{-1}; the basis for this variation is not well understood.

The above pyrophosphorolysis kinetics, however, do not distinguish between the two possible pathways for conversion of $E{\cdot}D_n + PP_i \rightarrow E'{\cdot}D_n{\cdot}PP_i$, either via an activated state $E'{\cdot}D_n$ or from an unactivated $E{\cdot}D_n{\cdot}PP_i$ complex. The question is

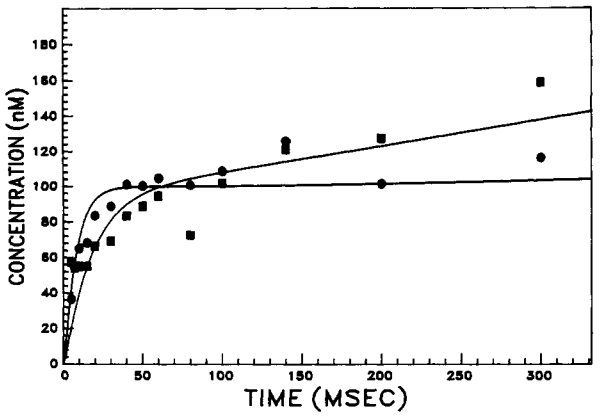

FIGURE 7: Pyrophosphate exchange kinetics. A preincubated solution of T7 DNA polymerase (100 nM) and 25/36-mer (200 nM) was mixed in two separate reactions with [γ-^{32}P]dTTP (10 μM) and with [γ-^{32}P]dTTP (10 μM) and PP$_i$ (5 mM) to initiate the reactions. The time course of [^{32}P]PP$_i$ formation was quantitated by charcoal columns as described under Materials and Methods. The curve (●) represents the time course of the reaction with no PP$_i$, and the curve (■) represents the time course of the reaction containing 5 mM PP$_i$. The solid lines were obtained by computer simulation to the mechanism shown in Scheme I and rate constants shown in Table II.

whether the conformational change precedes or follows the binding of PP$_i$ in the reverse reaction. The pyrophosphate exchange kinetics finally enabled us to resolve the pathway. Since the pyrophosphate exchange experiment is started from the forward direction, PP$_i$ can exchange either from the activated complex or from the unactivated complex, and therefore, depending on the mechanism, the observed pyrophosphate exchange rates in each case will be different and diagnostic of the pathway.

Kinetics of the Pyrophosphate Exchange Reaction. The pyrophosphate exchange reaction is also the reverse of the polymerization reaction and, in principle, it measures the same reaction as pyrophosphorolysis. Experimentally, while the pyrophosphorolysis reaction is started from E·D$_{n+1}$ complex and reacted with PP$_i$ to reverse the reaction, the pyrophosphate exchange reaction is started from E·D$_n$ complex and the elongated product E·D$_{n+1}$ is formed in situ in the presence of PP$_i$, which drives the reaction backwards. Consequently, if the conformational change (step 5, Scheme I) occurs before the release of PP$_i$, then the pyrophosphate exchange rates will be identical with the pyrophosphorolysis rates. On the other hand, if this conformational change occurs after PP$_i$ release, then the pyrophosphate exchange rates may be significantly greater than the pyrophosphorolysis rates.

The pyrophosphate exchange experiment was conducted as follows: T7 DNA polymerase (100 nM) was preincubated with 25/36-mer (200 nM) in the presence of 5 mM PP$_i$ in one reaction and in absence of PP$_i$ in the second reaction. The reaction was started by mixing the above solution with Mg^{2+}·[γ-^{32}P]dTTP in a rapid-quench instrument. The reactions were stopped by quenching with 0.3 M EDTA and the product [^{32}P]pyrophosphate was resolved from the [γ-^{32}P]-dTTP on charcoal columns. Figure 7 shows the time courses of [^{32}P]pyrophosphate production both in the presence and in the absence of unlabeled excess PP$_i$. In the absence of PP$_i$, the kinetics represent simply the burst of single-nucleotide addition as shown earlier but measured by PP$_i$ production rather than D$_{n+1}$. In the presence of PP$_i$, a slow phase following the burst was observed due to the pyrophosphate exchange reaction. The rate of the slow phase plotted as a function of increasing concentration of PP$_i$ (data not shown) gave a K_d of PP$_i$ binding equal to 3.0 ± 0.8 mM and a maximum exchange rate equal to 1.5 ± 0.2 s^{-1}, which are close to the rate and equilibrium constants describing the pyrophosphorolysis reaction. These results therefore support the pathway where the conformational change precedes PP$_i$ release, E·D$_n$ + PP$_i$ ⇄ E·D$_n$·PP$_i$ ⇄ E′·D$_n$·PP$_i$. A single set of rate constants for the reverse steps (Table II) was established by computer simulation to account for both the pyrophosphorolysis and pyrophosphate exchange kinetics.

Overall Equilibrium Constant. The overall equilibrium constant of enzyme bound 25/36-mer elongating to 26/36-mer was measured at several different PP$_i$ concentrations in the following manner. 5′-^{32}P-labeled 25/36-mer (50 nM) was preincubated with a 4-fold excess of T7 DNA polymerase (exo$^-$, 200 nM) in the presence of magnesium, and the reaction was initiated by mixing the complex with a solution containing a low concentration of dTTP (0.16 μM) and varying concentrations of PP$_i$ (0.5–4.0 mM) in separate reactions. The reactions were quenched after 5–30 s and analyzed by sequencing gel. The bands corresponding to the substrate 25-mer and the product 26-mer were quantitated, and the overall equilibrium constant of (1.0 ± 0.2) × 10^4 was calculated from the relationship K_{eq} = [26-mer][PP$_i$]/[25-mer][dTTP]. From the overall equilibrium constant and the measured K_ds of substrates, dNTP, and PP$_i$, the internal equilibrium constant, which is the product of $K_2K_3K_4$, was calculated as 100. The above experiments, however, provide no further constraints on the individual internal equilibrium constants. The pulse–chase experiments described below provided additional information to define the internal equilibrium constants.

Pulse–Chase Experiment. The following pulse–chase experiment allowed us to more accurately estimate the equilibrium constant of both the first conformational change step and the chemical step by measuring the flux of enzyme-bound radiolabeled dNTP after addition of a large excess of cold dNTP. Since the flux of accumulated radiolabeled dNTP bound to the enzyme is most sensitive to the rate constants k_{-2} and k_3 and the equilibrium constant of the chemical reaction, its measurement provided new information to define those steps and allowed us to finally solve the complete mechanism. The pulse–chase experiment was carried out by comparing the time courses of two independent experiments, both conducted by reacting E·25/36-mer (500 nM each) with Mg^{2+}·[α-^{32}P]dTTP (50 μM) in a rapid chemical quench-flow instrument. In one experiment the reaction was quenched with 1 N HCl, while in the other the reaction mixture was chased by the addition of cold dTTP (1.2 mM) for a fixed amount of time (20 s) sufficient for complete reaction of the enzyme-bound species, followed by stopping the reaction with 1 N HCl. Since the largest difference between the time courses of product formation between the HCl quench and the chase experiment was expected in the first few milliseconds, the experiment was carried out at lowered temperature (5 °C) in order to more accurately measure the difference. The resulting time courses are shown in Figure 8A. In the HCl quench experiment, the acid quenches all the enzyme-bound species, thus resulting in a small lag of product formation observed particularly at lowered temperature. On the other hand, when the reaction is chased with cold dTTP, each of the enzyme-bound species is allowed to partition both in the forward and the reverse directions, the flux in each direction being determined by the corresponding rate constants out of that ground state. In this experiment, the amount of labeled dTTP that partitions in the reverse direction gets diluted with cold dTTP and remains unobservable, while the amount that partitions in the forward direction is observed as an excess of

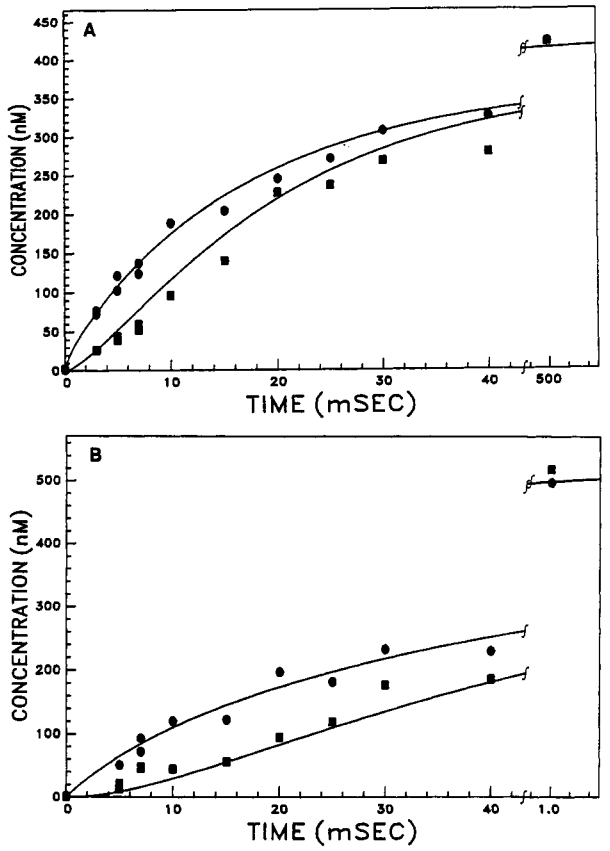

FIGURE 8: Pulse–chase experiment with dTTP and dTTP(αS). (A) The dTTP pulse–chase experiment was carried out comparing the kinetics of two experiments, one quenched with HCl (■) and the other chased with cold dTTP (●). Both the HCl quench and the dTTP chase experiments were carried out by mixing a preincubated solution of enzyme and 25/36-mer (500 nM each) with radiolabeled Mg^{2+}·dTTP (50 μM, ~20000 counts/pmol) for time intervals ranging from 3 to 500 ms at 5 °C. In the HCl quench experiment, the reactions were quenched with 1 N HCl, followed by denaturation with chloroform and neutralization with base. In the chase experiment, instead of quenching with acid, the reactions were chased with cold dTTP (1.2 mM) for 20 s, followed by quenching with HCl and neutralization. The time courses of labeled 26/36-mer formation were obtained by separating the labeled DNA from the unreacted dNTP by using Bio-Gel P-30 (Bio-Rad) gel-filtration columns. (B) The dTTP(αS) HCl quench (■) and chase experiments (●) were similarly carried out by using 420 nM of 25/36-mer, 500 nM of enzyme, 50 μM of [α-^{35}S]dTTP and chasing with 1.2 mM of cold dTTP from time intervals ranging from 3 ms to 1 s and analyzing the products by using gel-filtration columns.

labeled product. The time courses shown in Figure 8A suggest that a measurable amount of the hot dTTP is being chased in the forward direction to form labeled product, which is in excess to the amount formed after the HCl quench, particularly in the initial time period. At longer time periods, as expected, both experiments gave the same amount of product. Furthermore, 50% of the enzyme-bound dTTP reacts to form labeled product after being chased with cold dTTP. Since the binding of dTTP to the E·D complex is rapid, the observed flux is mainly due to the E′·D·N species that accumulates to a significant level during the reaction. The difference between the kinetics of product formation with HCl quench versus the chase experiment fits to a single set of rate constants, which are shown in Table II with k_{-2} equal to 100 s^{-1} and an equilibrium constant of the chemical reaction equal to 0.5. The same experiment was repeated with [α-^{35}S]dTTP, and the time courses of the acid quench versus the chase are shown in Figure 8B. A larger difference is seen in the [α-^{35}S]dTTP chase experiment due to its slower chemistry rate, which results in

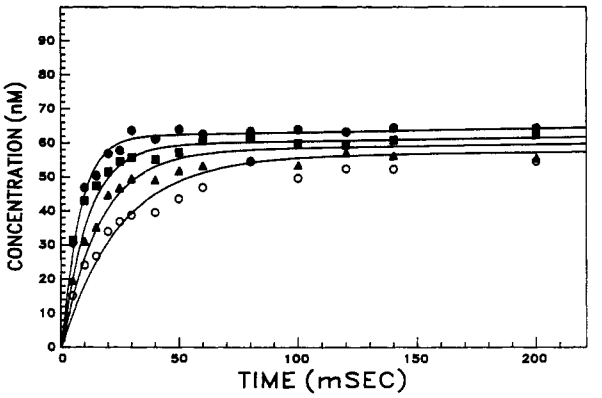

FIGURE 9: Inhibition of the single-turnover dTTP incorporation rate by inorganic PP_i. The reactions were conducted by mixing a solution of T7 DNA polymerase (100 nM), 5′-^{32}P-labeled 25/36-mer (100 nM), and various concentrations of PP_i (0–10 mM) with Mg^{2+}·dTTP (20 μM). The products were quantitated by sequencing gels. The curves represent (●), no PP_i; (■), 20 mM PP_i; (▲), 5.0 mM PP_i; and (○), 10 mM PP_i. The solid lines were calculated by computer simulation to the rate constants in Table II with PP_i binding to E·D_n to form E·D_n·PP_i with a K_i of 2.0 mM.

both a longer lag when quenched with HCl and an almost 60% flux of enzyme-bound [α-^{35}S]dTTP reacting to form product when chased with cold dTTP. The above experiments therefore allowed us to establish the complete mechanism of single dNTP addition.

PP_i and dTTP Are Competitive Inhibitors. The proposed kinetic pathway predicts that PP_i and the next correct nucleotide, dTTP, bind to the same form of the E·DNA complex. Consequently, the single-turnover rate of dTTP incorporation should be inhibited competitively by PP_i. The following experiment was designed to measure the inhibition constant of PP_i and consisted of reacting a preincubated complex of T7 DNA polymerase (50 nM), 5′-^{32}P-labeled 25/36-mer (100 nM), and various concentrations of PP_i (0–10 mM) with Mg^{2+}·dTTP (20 μM). The resulting time courses of 26/36-mer formation are shown in Figure 9. As predicted by the proposed mechanism, the single-turnover rate of dTMP incorporation decreased with increasing concentrations of pyrophosphate with a K_i of 2 mM, which is equal to its K_d. Interestingly, the amplitude of the burst also decreased gradually with increasing PP_i concentration as predicted by our model, due to the reversal of the chemical reaction with PP_i driving the reaction backwards.

Processive Polymerization. Knowledge of the kinetic pathway of a single nucleotide incorporation allows prediction of the pathway of processive polymerization. Being a replicative enzyme, T7 DNA polymerase is highly processive. Processivity, which is defined as the ratio of the polymerization rate to the dissociation rate, is therefore equal to 300/0.2 = 1500 at 20 °C for T7 DNA polymerase. The time course of processive DNA polymerization was investigated by using a slightly longer primer/template, 30/60-mer (Table I). By including only three dNTPs, the elongation of 30/60-mer was stopped at the 47/60-mer, simplifying the kinetic analysis. The experiment was carried out with a 2-fold excess of 30/60-mer (200 nM) over the polymerase (exo$^-$, 100 nM). Under these conditions, any elongated product that dissociates from the enzyme will be trapped by the excess of the starting DNA, assuring that the measured kinetics of elongation are due to a single binding event. The experiment was analyzed by sequencing gel electrophoresis, and the bands were quantitated by densitometry and integration of the peaks (Figure 10). The formation and disappearance of the intermediate product peaks were simulated to a mechanism consisting of a series of 17

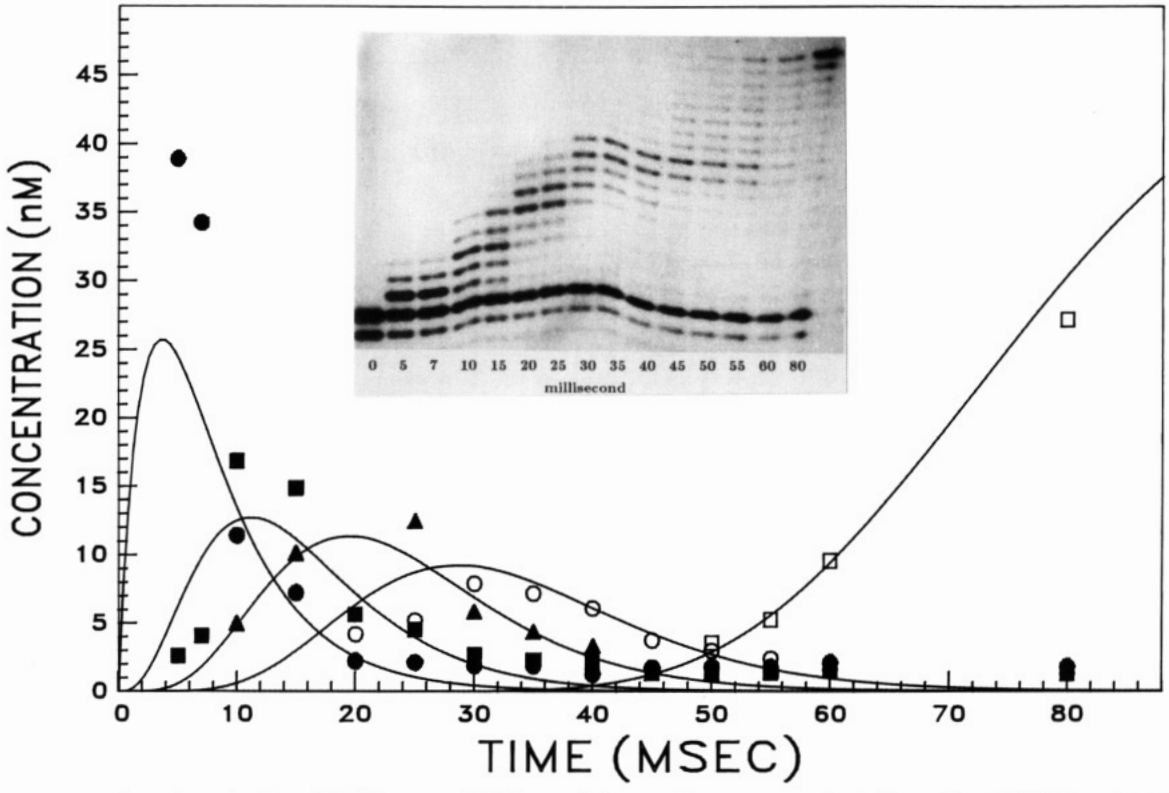

FIGURE 10: Processive polymerization of 30/60-mer to 47/60-mer. The experiment was conducted by mixing T7 DNA polymerase (exo$^-$, 50 nM) and 5′-^{32}P-labeled 30/60-mer (100 nM) with dTTP, dATP, and dCTP (100 μM each) in magnesium buffer. The reactions were quenched with 0.3 M EDTA and analyzed by sequencing gel electrophoresis. The curves (●), 31-mer; (■), 33-mer; (▲), 35-mer; (○), 37-mer; and (□), 47-mer were obtained by quantitating the intermediate products from a densitometric scan of the autoradiogram. The solid lines are curves obtained from computer simulation using a mechanism consisting of a series of seventeen single-nucleotide incorporation pathways with the following net rate constants for formation of each intermediate species: 31-mer at 390 s^{-1}, 32-mer at 180 s^{-1}. 33-mer at 345 s^{-1}, 34-mer at 225 s^{-1}, 35-mer at 320 s^{-1}, 36-mer at 190 s^{-1}, and 37-mer at 255 s^{-1}.

single nucleotide incorporation events, with rate constants of 270 ± 80 s^{-1}. Because of the experimental uncertainty in measuring the very fast 31/60-mer formation and disappearance, the fit of the experimental amplitude to the simulated curve is poor. However, when the same experiment was carried out at lower temperature (5 °C, data not shown), the observed rates were 2.5 times slower and the amplitudes of 31/60-mer as well as the other intermediate products lay close to the predicted curves.

Complete Characterization of the Mutant Enzyme. The exo$^-$ mutant of the polymerase was prepared by site-directed mutagenesis of two amino acid residues, D5A and E7A, which completely eliminated the polymerase-associated 3′–5′ exonuclease activity as demonstrated below.

(*A*) *Exonuclease on Duplex "Natural" DNA.* We began our studies by comparing the exonuclease activity of the mutant with that of the wild-type enzyme on natural DNA (calf thymus DNA, data not shown). An arbitrary but consistent concentration of randomly labeled calf thymus DNA was incubated with varying concentrations of wild-type or mutant enzyme from 0.1 nM up to 5 μM. The incubation time was fixed at 5 min, and the fraction of radiolabel remaining in the DNA substrate was quantitated by DE81 filter binding assays. Under these reaction conditions, less than 1 nM wild-type enzyme was required to excise half the counts in 5 min. In contrast, concentrations as high as 5 μM of the mutant enzyme did not give detectable amounts of exonuclease activity towards duplex DNA.

(*B*) *Exonuclease on Single-Stranded DNA.* Because the rate of excision of single-stranded DNA is higher than that for duplex DNA (data not shown), we sought to increase the sensitivity of our exonuclease assay by switching to a single-stranded substrate. Using single-stranded 20-mer at 50 nM with a 10-fold excess of enzyme, we measured a linear rate of excision of 8×10^{-5} s^{-1} (data not shown). The comparable rate of excision for the wild-type enzyme was ≥100 s^{-1}. Thus the exonuclease activity of the mutant was reduced >10^6-fold.

(*C*) *Exonuclease on Mismatched DNA.* We then assayed the rate of excision of a single mismatch at the 3′-terminus of a duplex primer/template system (25A/36-mer). At 50 nM DNA and 500 nM enzyme, the rate of excision was measured as 4×10^{-5} s^{-1} (data not shown) as compared with to a rate of 100 s^{-1} for the wild-type enzyme (Donlin et al., 1990).

(*D*) *Kinetic Constants for the Polymerization Reaction.* The dissociation constants for DNA and dTTP and the maximum rate of incorporation (k_p) for the mutant enzyme were determined exactly as described above for the wild-type enzyme (data not shown). These values are reported in Table III, which summarizes all the kinetic measurements made on the mutant in comparison of the wild type. This comparison establishes unambiguously that the wild-type enzyme and the mutant enzyme catalyze DNA synthesis by the same mechanism governed by the same set of kinetic and thermodynamic parameters at each elementary step throughout the kinetic pathway.

Discussion

DNA polymerases, in general, are faced with the problem of catalyzing the incorporation of all four dNTPs with the same efficiency and at the same time discriminating against the other three dNTPs during each cycle of nucleotide incorporation. Studies in this paper define the kinetics and thermodynamics of correct nucleotide incorporation catalyzed

by T7 DNA polymerase. The accompanying papers define the kinetics of misincorporation (Wong et al., 1991) and of proofreading (Donlin et al., 1991).

Our goal in investigating the mechanism of T7 DNA polymerase was to identify and quantitate the elementary steps leading to a correct nucleotide incorporation pathway. The steady-state kinetics of single-nucleotide incorporation are remarkably uninformative, providing only the rate of DNA dissociation from the enzyme—the slowest step under those conditions (Figure 1A). This is not unexpected for a processive DNA polymerase where the dissociation rate of the polymerase from the DNA must be slow in order for the polymerase to incorporate thousands of bases without dissociating from the DNA. Therefore, the general conclusion from these studies is that the k_{cat} measured from steady-state turnover involving the addition of one or a few dNTPs is dominated by the slow dissociation rate of the DNA from the enzyme rather than the real polymerization rate. This holds true for all processive polymerases and for replicative complexes, such as phage T4 and *E. coli* polymerase III (McHenry, 1988), and has been observed even for polymerases with moderate processivity (50–100), such as the Klenow fragment of Pol I (Kuchta et al., 1987).

The transient-state time course of single-nucleotide incorporation, however, provides new mechanistic information. Under conditions where the DNA is present in 3-fold excess of the polymerase concentration, the pre-steady-state time course of dTMP incorporation into 25/36-mer biphasic (Figure 1B); the burst of product formation is due to the very fast first incorporation of dNMP, while the slow exponential gives the rate of subsequent turnovers, which are limited by the dissociation of the DNA from the enzyme. The amplitude of the burst corresponds to the amount of complexed E·DNA species in the preincubated solution (E + DNA $\rightleftarrows$ E·DNA), and the burst rate corresponds to the rate of the slowest step during the single-nucleotide incorporation reaction, E·25/36-mer $\rightarrow$ E·26/36-mer. A complete study of the DNA concentration dependence on the amplitude and the dTTP concentration dependence on the burst rate provided measurements of the true dissociation constants of 25/36-mer and dTTP equal to 18 nM and 18 μM, respectively. Furthermore, the maximum rate of single dTMP incorporation, determined to be 300 s^{-1}, was found to correspond to a step other than chemistry because of a very small phosphothioate elemental effect. An elemental effect of 3.1, in fact, suggested that the chemical reaction occurred at a rate greater than 9000 s^{-1}. On the basis of these results, we have assigned the 300 s^{-1} rate-limiting step to a conformational change (E·D_n·dNTP $\rightleftarrows$ E′·D_n·dNTP) occurring before chemistry. Interestingly, the kinetic pathway of the Klenow fragment also contains a rate-limiting conformational step, which, however, occurs at a rate 6 times slower (50 s^{-1}) than that of T7 DNA polymerase (300 s^{-1}).

On the basis of our studies with correct and incorrect nucleotide incorporations, we propose the conformational change as part of an "induced-fit" type of mechanism (Wong et al., 1991). Accordingly, the binding energy of a correct dNTP is utilized in driving the 300 s^{-1} rate-limiting conformational change, which results in aligning the reactive groups of the substrates and the enzyme to facilitate the very fast phosphodiester bond formation reaction. As described in more detail in the accompanying paper (Wong et al., 1991), the enzyme utilizes this type of mechanism in selecting one of the four dNTP substrates during each nucleotide incorporation cycle. Presently, it is not possible to assign this conformational change to a specific structural rearrangement of the enzyme–substrate complex because of the lack of structural data.

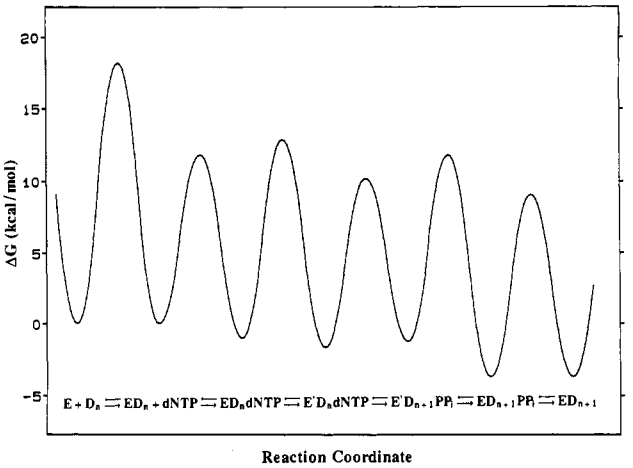

FIGURE 11: Free energy profile for T7 DNA polymerase. The free energy changes for elongation of 25/36-mer to 26/36-mer by dTMP addition were calculated from the rate constants shown in Table II. The concentrations of the substrates and products 25/36-mer, dTTP, and PP_i were set equal to 20 nM, 100 μM, and 2 mM, respectively. The free energy was calculated as $\Delta G^{\ddagger} = RT[\ln(kT/h) - \ln(k_{obs})]$ kcal/mol, where k is the Boltzmann constant, T is 293 K, h is Planck's constant, and k_{obs} is the first-order rate constant.

DNA polymerization is a reversible reaction, and by studying the single-turnover kinetics of pyrophosphorolysis and the steady-state rate of the pyrophosphate exchange reaction, it was possible to elucidate the complete pathway of DNA polymerization. In practice, it was difficult to measure the kinetics of the reverse reaction independent of the exonuclease reaction of T7 DNA polymerase. Hence, we prepared an exo$^-$ mutant of the polymerase. The single-turnover kinetics of the pyrophosphorolysis reaction, the pyrophosphate exchange reaction, and the pulse–chase experiment measured by using this exo$^-$ mutant led to the solution of the complete mechanism of single-nucleotide incorporation.

Two-Step Model for Correct dNMP Incorporation. The mechanism of DNA polymerization consists of a series of single dNMP incorporation reactions. A nucleotide incorporation event begins by the binding of a dNTP to the E·DNA complex. The binding of a correct dNTP induces a conformational change, which results in formation of a "tight" ternary complex (E·D_n·dNTP $\rightleftarrows$ E′·D_n·dNTP). The chemical reaction that follows is fast and results in formation of a tightly bound enzyme–product complex (E′·D_n·dNTP $\rightleftarrows$ E′·D_{n+1}·PP_i); this complex then needs to undergo a second conformational change, which would relax the tightly bound enzyme–product complex (E′·D_{n+1}·PP_i $\rightleftarrows$ E·D_{n+1}·PP_i). This second conformational change, we propose, corresponds to the additional step that we have identified in the DNA polymerase pathway. In the forward reaction, this step is a relaxation step facilitating PP_i release and allowing translocation of the DNA for the next cycle of polymerization. On a qualitative basis, therefore, the proposed mechanism suggests that the E·DNA complex periodically fluctuates between a loose binding and a tight binding state such that the binding and release of the substrates and products as well as the linear diffusion or sliding of the DNA would occur in the loose binding state while the chemical reaction would occur in the tight binding state.

The major difference between the kinetic pathway of the Klenow fragment and that of the T7 DNA polymerase is apparently the absence of this second conformational change or the relaxation step in Klenow. This is evidenced by the reported biphasic nature of the pyrophosphorolysis kinetics (Kuchta et al., 1987). The basis for the difference in the

kinetic pathways of the two polymerases requires further investigation.

Free Energy Profile. The free energy diagram (Figure 11) shows the kinetic and the thermodynamic pathway of a single-nucleotide incorporation cycle during processive DNA polymerization. The free energies were calculated from the elementary rate constants measured for dTMP addition to DNA, 25/36-mer, catalyzed by T7 DNA polymerase, by using the following concentrations of the substrates and products: [DNA] = 20 nM, which is equal to its K_d, [dNTP] = 100 μM, and [PP_i] = 2 mM, concentrations of both being close estimates to the physiological concentrations. The overall free energy change for the reaction would be base dependent, and for dTMP incorporation in 25/36-mer the overall free energy change is equal to 3.97 kcal/mol. The most striking feature of the free energy diagram is the largest activation barrier corresponding to the dissociation of the DNA from the enzyme. However, during processive DNA synthesis, when the enzyme remains bound to the DNA, the induced-fit conformational change becomes rate limiting. It is interesting that the second conformational change following the chemical step occurs with the largest ground-state free energy change (2.37 kcal/mol). The large activation barrier for this step in the reverse direction essentially makes both pyrophosphorolysis and the reverse translocation of the DNA highly unfavorable, thus preventing pyrophosphorolysis of the DNA and facilitating unidirectional sliding of the polymerase on the DNA.

Derivation of Individual Rate Constants for Single-Nucleotide Addition. The rate constants shown in Table II are either directly measured or estimated from computer simulation of all the experiments described in this paper to a single model by the computer simulation program KINSIM. The simulation was carried out by a trial and error process to fit the data, and the final solution was optimized by nonlinear regression analysis as described by Zimmerlie and Frieden (1989). The fit was constrained by the directly measured kinetic constants, which include the dissociation constants of DNA, dNTP, and PP_i, the maximum rate of nucleotide incorporation equal to 300 s^{-1}, the maximum rate of pyrophosphorolysis, the flux of product formation during the pulse–chase experiment, and the overall equilibrium constant of 10000 (product of $K_1K_2K_3K_4K_5$). The rate constants for the conformational changes and the chemical step are constrained by the internal equilibrium constant of 100 estimated from the overall equilibrium constant of 10000 and the K_ds for dNTP and PP_i binding steps. Furthermore, the pulse–chase experiment constrained the equilibrium constant of the chemical step to be close to 0.5 and the reverse rate constant of the first conformational step to 100 s^{-1}. The dissociation rate constants of both dNTP and PP_i are very high and can be varied over a range with little effect on the overall fit to the data; hence, a lower limit of 1000 s^{-1} is reported for each of the rate constants. The second-order binding rates for dNTP and PP_i shown in Table II were calculated from the experimentally measured K_ds and the 1000 s^{-1} dissociation rate constants for each substrate. The slower rate of dTTP(αS) incorporation with an elemental effect of 3 provided a lower limit for the rate of the chemical steps, k_3 and k_{-3}, and assuming an elemental effect between 60 and 100, chemistry occurs with a forward rate constant of 9000 s^{-1} and a reverse rate constant of 18000 s^{-1}. The rates of the conformational changes in the forward direction, k_2 = 300 ± 30 s^{-1} and k_3 = 1200 ± 280 s^{-1}, were estimated from best fits to the forward polymerization kinetics, while the rate of the reverse reaction, k_{-4} = 18 ± 0.5 s^{-1}, was derived from the pyrophosphorolysis kinetics of both the wild-type and the exo$^-$ mutant enzymes.

An Alternative Mechanism for Single-Nucleotide Addition. We must consider that *most* of the measured kinetics for single-nucleotide addition would also be consistent with an alternative mechanism with a different set of a rate constants in which the rate-limiting conformational change occurred only after the chemical step with an unfavorable equilibrium constant for chemistry:

$$E \underset{k_{off}}{\overset{k_{on}[D_n]}{\rightleftharpoons}} E{\cdot}D_n \underset{k_{-1}}{\overset{k_1[N]}{\rightleftharpoons}} E{\cdot}D_n{\cdot}N \underset{k_{-2}}{\overset{k_2}{\rightleftharpoons}} E'{\cdot}D_{n+1}{\cdot}P \underset{k_{-3}}{\overset{k_3}{\rightleftharpoons}} E{\cdot}D_{n+1}{\cdot}P \underset{k_{-4}[P]}{\overset{k_4}{\rightleftharpoons}} E{\cdot}D_{n+1}$$

Because the rate-limiting step (k_3) in this mechanism occurs after chemistry, one would expect biphasic product formation within the first turnover due to the rapid reaction to establish the internal equilibrium for the chemical step. The amplitude of the fast incorporation should be a function of the internal equilibrium for the chemical step (k_2/k_{-2}). The fact that no such fast phase was observed could be explained by a highly unfavorable equilibrium for the chemical step in the forward direction, resulting in a fast phase that is too small to be detected by our method. Since a reasonable limit of detection for the amplitude of the fast phase, at least at lowered temperature, can be placed around 5%, an upper limit of 0.05 can be placed for the chemical equilibrium. With the above assumed limit, one can then calculate the rates of the individual steps required to explain the 300 s^{-1} rate in the forward direction and 1 s^{-1} in the reverse direction with an internal equilibrium constant equal to 100. Accordingly, this would require a lower limit of 6000 s^{-1} for the rate of the conformational change in the forward direction (k_3). The pyrophosphorolysis kinetics, on the other hand, places an upper limit on the rate of the reverse conformational change (k_{-3}) that is equal to 3 s^{-1}. The lack of a full elemental effect predicts the rate of the chemical reaction in the forward direction (k_2) as 10000 s^{-1} and that in the reverse direction (k_{-2}) as 2×10^5.

This alternate mechanism accounts for the majority of the experimental results presented in this paper and for data previously presented in studies on Pol I Klenow. However, it is excluded by the pulse–chase experiments designed to detect the E'·DNA·dNTP complex. The significant buildup and forward kinetic partitioning of the enzyme-bound dNTP species forms the basis for distinguishing the two mechanisms by requiring the additional enzyme state. These observations and the unreasonably high rates required by the alternative mechanism allows us to rule it out. Only the complete mechanism shown in Scheme I can account for all of the data.

Sequence Dependence of the Rate Constants. The rate and the equilibrium constants proposed for incorporation or pyrophosphorolysis of dTTP into the 25/36-mer are subject to subtle variations depending on the sequence of the DNA. The rate of the pyrophosphorolysis reaction, for instance, varied over an order of magnitude depending on the base removed and the 3′-base sequence of the DNA primer/templates, as shown in Table IV. This larger dependence of the reverse reaction on the base sequence explains the discrepancy between pyrophosphorolysis and pyrophosphate exchange rates reported earlier in the literature by Deutscher and Kornberg [1969; see also Kornberg (1980, 1982)], which implied an activated enzyme–DNA complex. The observed higher rate of the pyrophosphate exchange reaction compared to the pyrophosphorolysis reaction can now be understood due to the mixture of 3′-bases of the DNA primer/templates used in their experiments. The difference will be accentuated by the

steady-state nature of their measurements, which would give an average rate for the pyrophosphate exchange reaction faster than the pyrophosphorolysis rate measured under the same conditions.

The sequence dependence of the forward reaction is clearly seen in the experiment where the processive synthesis of 30/60-mer to 47/60-mer was quantitated (Figure 10). The time dependence of appearance and disappearance of each elongated DNA species could be fit by varying the rate constants used for each dNTP addition over a range of only 270 $\pm$ 80 s^{-1}, close to the value measured for dTTP addition. The rate constants and equilibrium constants for addition of each of the four dNTPs is a function of not only the particular dNTP added but also the sequence of the neighboring bases. Hence, a detailed investigation of the sequence dependence of dNTP addition could provide quantitation of both the free energies of base pairing as well as the stacking interactions with the neighboring base pairs. Nonetheless, the relatively small variation in rate constants for individual nucleotides along the sequence does not alter the generality of the conclusions from these studies. Rather, these results point to the necessity to perform all experiments with a single oligonucleotide to allow for a quantitatively consistent and complete analysis of the reaction pathway. Hence, while establishing the mechanism of correct or incorrect nucleotide incorporations, it is critical to conduct all experiments with the same nucleotide added and removed by the polymerization and pyrophosphorolysis or pyrophosphate exchange reactions, respectively, at the same position on the DNA, in order to achieve a thermodynamically consistent set of rate constants. This has not been achieved previously in studies with any DNA polymerase.

Exonuclease-Deficient Mutant of T7 DNA Polymerase. Our primary interest in constructing the mutant stems from the need for an exonuclease-deficient enzyme in order to complete our kinetic study of T7 DNA polymerase where the exonuclease activity interferes severely with the measurements of several crucial kinetic parameters. While an exonuclease-deficient mutant of T7 DNA polymerase already exists on the market (Tabor & Richardson, 1989), we felt that it is of utmost importance to us that the polymerase region of our mutant be unaffected by the mutations in the exonuclease site. For this reason, we opted to make a minimal change of two amino acid substitutions instead of the 28 amino acid deletion mutation of Tabor and Richardson.

Unfortunately, beyond reporting that the mutant exhibits a 10^6-fold reduction in exonuclease activity, we are unable at present to provide any direct evidence for the mechanism of exonuclease inactivation. Presumably we have removed two putative metal binding ligands, on the basis of structural analogy to Pol I. X-ray and mutagenic data on Pol I (Joyce & Steitz, 1987; Derbyshire et al., 1988) indicate that the exonuclease site contains two metal binding sites and that Asp-355 and Glu-357, the amino acids in Pol I analogous to Asp-5 and Glu-7 in T7, provide two key ligands for metal binding. Substitutions at these two positions by alanines result in the loss of both binding sites. By direct comparison, it is assumed that the mutations reported here would have a similar effect of disrupting metal binding at the exonuclease site. Efforts are currently underway to confirm this by spectroscopic means.

Amino acid sequence homology data divide DNA polymerases into two general "families". T7 DNA polymerase belongs in the *E. coli* Pol I like family and shares significant sequence homology with polymerases from *Streptococcus pneumoniae* (López et al., 1989), *Thermus aquaticus* (Lawyer et al., 1989), and bacteriophage T5 (Leavitt & Ito, 1989). A second family of α-like polymerases spans a diverse range of sources ranging from bacteriophages T4, PRD1, $\phi 29$, and VZV to eukaryotic viruses and Pol I from *Saccharomyces cerevisiae*. Although the overall amino acid sequences of polymerase from the two different families are not greatly homologous, several significant similarities have been noted in the most recent studies (Reha-Krantz, 1988a,b; Bernad et al., 1989; Leavitt & Ito, 1989). First, in enzymes with associated 3′–5′ exonuclease activities, highly conserved segments homologous to segments in the exonuclease domain of Klenow can be found at the N-terminal region. Secondly, in enzymes where the associated 3′–5′ exonuclease activity resides on a separate subunit of the holoenzyme replication complex such as *E. coli* Pol III, the exonuclease subunits are also found to contain these highly conserved segment. Together, these two observations suggests strongly that (1) the 3′–5′ exonuclease domains of polymerases are highly homologous in discrete regions representing evolutionarily conserved structure–function motifs and (2) the exonuclease domain and the polymerase domain are separate and distinct even in enzymes that carry both activities on the same subunit.

The results of our mutagenesis provide direct evidence in support of these hypotheses. We have replaced two of the absolutely conserved amino acids in T7 DNA polymerase in accord with homology data and have found the resultant mutant to be almost completely devoid of exonuclease activity. While ours is not the first example of the effect of mutations at these two residues, we have provided the most complete characterization of the kinetic consequences of the mutations. By solving the kinetic mechanism for polymerization in the mutant enzyme, we have established by direct comparison with the wild-type enzyme that the polymerase domain is structurally and functionally distinct from the exonuclease domain.

This study defines the kinetics and thermodynamics of the reaction pathway leading to the processive incorporation of correctly base-paired dNTPs and provides the basis for subsequently analysis of the kinetics of misincorporation and proofreading to establish the kinetic basis for DNA polymerase fidelity in the accompanying two papers.

ACKNOWLEDGMENTS

We thank Steve Benkovic for encouraging us to pursue studies on T7 DNA polymerase.

Registry No. 25/36-mer, 130522-93-9; 30/60-mer, 130522-92-8; dTTP, 365-08-2; Pol I, 9012-90-2; exodeoxyribonuclease, 79393-91-2; pyrophosphate, 14000-31-8.

REFERENCES

Anderson, K. S., Sikorski, J. A., & Johnson, K. A. (1988) *Biochemistry 27*, 7395–7406.

Barshop, B. A., Wrenn, R. F., & Frieden, C. (1983) *Anal. Biochem. 130*, 134–145.

Benkovic, S. J., & Schray, K. J. (1971) *Enzymes (3rd Ed.) 8*, 20a.

Bernad, A., Blanco, L., Lázaro, J. M., Martín, G., & Salas, M. (1989) *Cell 59*, 219–222.

Boosalis, M. S., Petruska, J., & Goodman, M. F. (1987) *J. Biol. Chem. 262* (30), 14689.

Brutlag, D., & Kornberg, A. (1972) *J. Biol. Chem. 247*, 241–248.

Bryant, F. R., Johnson, K. A., & Benkovic, S. J. (1983) *Biochemistry 22*, 3537–3546.

Derbyshire, F., Freemont, P. S., Sanderson, M. R., Beese, L., Friedman, J. M., Joyce, C. M., & Steitz, T. A. (1988) *Science 240*, 199–201.
Deutscher, M. P., & Kornberg, A. (1969) *J. Biol. Chem. 244*, 3019–3028.
Donlin, M. J., Patel, S. S., & Johnson, K. A. (1991) *Biochemistry* (third of three papers in this issue).
Fersht, A. (1985) *Enzyme Structure and Mechanism*, 2nd ed., p 363, W. H. Freeman & Co., New York.
Fuller, C. W., & Richardson, C. C. (1985a) *J. Biol. Chem. 260*, 3185–3196.
Fuller, C. W., & Richardson, C. C. (1985b) *J. Biol. Chem. 260*, 3197–3206.
Hopfield, J. J. (1974) *Proc. Natl. Acad. Sci. U.S.A. 71*, 4135.
Huber, H. E., Tabor, S., & Richardson, C. C. (1987) *J. Biol. Chem. 262*, 16224–16232.
Johnson, K. A. (1983) *J. Biol. Chem. 258*, 13825–13832.
Johnson, K. A. (1986) *Methods Enzymol. 134*, 677–705.
Joyce, C. M., & Steitz, T. A. (1987) *Trends Biochem. Sci. 12*, 288–292.
Kornberg, A. (1980) *DNA Replication*, W. H. Freeman & Co., San Francisco, CA.
Kornberg, A. (1982) *Supplement to DNA Replication 1980*, W. H. Freeman & Co., San Francisco, CA.
Kuchta, R. D., Mizrahi, V., Benkovic, P. A., Johnson, K. A., & Benkovic, S. J. (1987) *Biochemistry 26*, 8410–8417.
Kuchta, R. D., Benkovic, P. A., & Benkovic, S. J. (1988) *Biochemistry 27*, 6716–6725.
Kunkel, T. A., Beckman, R. A., & Loeb, L. A. (1986) *J. Biol. Chem. 261*, 13610–13616.
Lawyer, F. C., Stoffel, S., Saiki, R. K., Myambo, K., Drummond, R., & Gelfund, D. H. (1989) *J. Biol. Chem. 264*, 6427–6437.
Leavitt, M. C., & Ito, J. (1989) *Proc. Natl. Acad. Sci. U.S.A. 86*, 4465–4469.
Lin, T.-C., Rush, J., Spicer, E. K., & Konigsberg, W. H. (1987) *Proc. Natl. Acad. Sci. U.S.A. 84*, 7000–7004.
Litman, R. M. (1968) *J. Biol. Chem. 243*, 6222–6233.
Loeb, L. A., & Kunkel, T. A. (1982) *Annu. Rev. Biochem. 52*, 429–457.
López, P., Martínez, S., Díaz, A., Espinosa, M., & Lacks, S. A. (1989) *J. Biol. Chem. 264*, 4255–4263.
Lunn, C. A., Kathju, S., Wallace, B. J., Kushner, S. R., & Pigiet, V. (1984) *J. Biol. Chem. 259*, 10469–10474.
Maniatis, T., Fritsch, E. F., & Sambrook, J. (1982) *Molecular Cloning, A Laboratory Manual*, Cold Spring Harbor Laboratory, Cold Spring Harbor, NY.
McHenry, C. S. (1988) *Annu. Rev. Biochem. 57*, 519–550.
Mizrahi, V., Henrie, R. N., Marlier, J. F., Johnson, K. A., & Benkovic, S. J. (1985) *Biochemistry 24*, 4010–4018.
Modrich, P., & Richardson, C. C. (1975) *J. Biol. Chem. 250*, 5515–5522.
Ninio, J. (1975) *Biochemie 57*, 587.
Reha-Krantz, L. J. (1988a) in *DNA Replication and Mutagenesis* (Moses, R. E., & Summers, W. C., Eds.) p 34, American Society for Microbiology, Washington, DC.
Reha-Krantz, L. J. (1988b) *J. Mol. Biol. 202*, 711.
Reutimann, H., Sjoberg, B. M., & Holmgren, A. (1985) *Proc. Natl. Acad. Ser. U.S.A. 82*, 6793=6787.
Richardson, C. C., Beauchamp, B. B., Huber, H. E., Ikeda, R. A., Myers, J. A., Nakai, H., Rabkin, S. D., Tabor, S., & White, J. (1987) *DNA Replication and Recombination*, pp 151–171, Alan R. Liss, Inc., New York.
Stanssens, P., Opsomer, C., McKeown, Y. M., Kramer, W., Zabeau, M., & Fritz, H.-J. (1989) *Nucleic Acids Res. 17*, 4441–4454.
Tabor, S., & Richardson, C. C. (1989) *J. Biol. Chem. 264*, 6447–6458.
Tabor, S., Huber, H. E., & Richardson, C. C. (1987) *J. Biol. Chem. 262*, 16212–16223.
Wong, I., Patel, S. S., & Johnson, K. A. (1991) *Biochemistry* (second of three papers in this issue).
Zimmerlie, C. T., & Frieden, C. (1989) *Biochem. J. 258*, 381–387.